Molecular Cancer

RESEARCH

Open Access

Sulindac (K-80003) with nab-paclitaxel and gemcitabine overcomes drug-resistant pancreatic cancer

Cheng-Ke Xie[1,2†], Cheng-Yu Liao[1,2,3†], Hong-Yi Lin[1,2†], Yong-Ding Wu[1,2†], Feng-Chun Lu[10], Xiao-Xiao Huang[1,2,3], Zu-Wei Wang[1,2,3], Ge Li[4], Cai-Feng Lin[1,2,3], Jian-Fei Hu[1,2], Yin-Hao Chen[1,2], Qiao-Wei Li[1,5,6], Li-Qun Chen[7,9*], Hui-Xing Chen[4,8*] and Shi Chen[1,2,3,5,6*]

Abstract

The Nab-paclitaxel combined with gemcitabine (AG) regimen is the main chemotherapy regimen for pancreatic cancer, but drug resistance often occurs. Currently, the ability to promote sensitization in drug-resistant cases is an important clinical issue, and the strategy of repurposing conventional drugs is a promising strategy. This study aimed to identify a classic drug that targets chemotherapy resistance's core signaling pathways and combine it with the AG regimen to enhance chemosensitivity. We also aimed to find reliable predictive biomarkers of drug combination sensitivity. Using RNA sequencing, we found that abnormal PI3K/Akt pathway activation plays a central role in mediating resistance to the AG regimen. Subsequently, through internal and external verification of randomly selected AG-resistant patient-derived organoid (PDO) and PDO xenograft models, we discovered for the first time that the classic anti-inflammatory drug sulindac K-80003, an inhibitor of the PI3K/Akt pathway that we focused on, promoted sensitization in half (14/28) of AG-resistant pancreatic ductal adenocarcinoma cases. Through RNA-sequencing, multiplex immunofluorescent staining, and immunohistochemistry experiments, we identified cFAM124A as a novel biomarker through which sulindac K-80003 promotes AG sensitization. Its role as a sensitization marker is explained via the following mechanism: cFAM124A enhances both the mRNA expression of cathepsin L and the activity of the cathepsin L enzyme. This dual effect stimulates the cleavage of RXRα, leading to large amounts of truncated RXRα, which serves as a direct target of K-80003. Consequently, this process results in the pathological activation of the PI3K/Akt pathway. In summary, our study provides a new treatment strategy and novel biological target for patients with drug-resistant pancreatic cancer.

†Cheng-Ke Xie, Cheng-Yu Liao, Hong-Yi Lin and Yong-Ding Wu contributed equally to this work, and are considered as first author.

*Correspondence:
Li-Qun Chen
lqchen@fzu.edu.cn
Hui-Xing Chen
chenhuixing@163.com
Shi Chen
wawljwalj@163.com

Full list of author information is available at the end of the article

Introduction

Pancreatic ductal adenocarcinoma (PDAC) is one of the most lethal malignancies, with most patients having advanced disease at the time of diagnosis [1, 2]. Chemotherapy is the main treatment strategy for advanced PDAC, capable of transforming initially unresectable PDAC into resectable cancer [3, 4]. Due to the toxic side effects of the fluorouracil plus irinotecan plus oxaliplatin plus leucovorin (FOLFIRINOX) regimen, the Nab-paclitaxel plus gemcitabine regimen (AG regimen) is considered the best option in Asia [5, 6]. Nonetheless, the emergence of primary resistance to the AG regimen poses a significant clinical challenge, affecting approximately 40–60% of patients [7]. Currently, most studies focus on screening which patients are suitable for AG chemotherapy [8]. However, new methods to achieve chemotherapy sensitization in patients resistant to the AG regimen are overlooked. Recent research tried to combine immunotherapy with an AG regimen, but the results were unsatisfactory due to the low responsiveness of PDAC to immunotherapy [9, 10]. Therefore, the development of clinically effective AG re-sensitization therapies is an important clinical challenge.

Signaling pathway activation is closely related to chemotherapy resistance [11, 12]. The classic PI3K/Akt pathway is the core pathway among various tumor-related signaling pathways [13, 14], and its abnormal activation commonly detected in PDAC cases can greatly promote PDAC chemotherapy resistance [12, 15]. Therefore, using a combination of inhibitors targeting this pathway is a potential strategy to achieve chemotherapy sensitization. Previous studies have shown that chemotherapy combined with PI3K/Akt pathway inhibitors (e.g., Everolimus, BKM120, and Duvelisib) is an effective treatment strategy for breast cancer, head and neck squamous cell carcinoma, and non-Hodgkin lymphoma [16–18]. Preclinical studies showed that chemotherapy combined with PI3K/Ak/mTOR inhibitors (Everolimus and Sirolimus) may improve treatment efficacy for GEM-resistant PDAC cases [19–21]. However, clinical trial results for Everolimus did not show anti-tumor effects in patients with GEM-refractory metastatic PDAC [22], and another clinical study showed strong grade 3–4 adverse reactions during Everolimus administration [23]. In a phase II study of Sirolimus combined with GEM for the treatment of advanced PDAC, although 34.6% of patients achieved partial response, it greatly increased the risk of bone marrow suppression and infection [24]. Therefore, currently, in clinical practice, the use of the combination strategy involving PI3K/Akt pathway inhibitor-sensitizing chemotherapy is very limited. The search for safe and reliable PI3K/Akt pathway inhibitors is important in sensitizing PDAC to chemotherapy.

"Conventional drug in new use" is an important strategy for research and treatment of diseases at this stage, because a large amount of data supports drug safety with this strategy [25–27]. Our team previously focused on sulindac K-80003, a derivative of the clinical anti-inflammatory drug sulindac. As an inhibitor of the PI3K/Akt pathway, it has more reliable biological safety and precise targeting [28], as demonstrated in studies related to hepatocellular carcinoma and colorectal cancer [28, 29]. However, its potential therapeutic effects and whether sulindac K-80003 can promote the sensitization of pancreatic cancer to the AG regimen on PDAC are unknown. For the first time, we investigated a combination of sulindac K-80003 with the AG regimen in patient-derived organoid (PDO) and PDO xenograft (PDOX) treatment models from PDAC patients and demonstrated a positive therapeutic response. Given this promising finding, we sought to identify biomarkers to predict which patients may benefit from sulindac K-80003 combination therapy. Based on the characteristics of non-coding circular RNA (circRNA), which include a stable structure, a long half-life, and easy detection [30, 31], we have identified a circRNA as a potential biomarker for sulindac K-80003-promoted AG sensitization [32, 33]. Previous studies have reported that circRNAs can be highly powerful predictors of chemotherapy sensitivity, such as circ-DOPEY2 for cisplatin chemotherapy in esophageal cancer [34] and circ-CREIT for DOX in breast cancer [35]. Based on these studies we hypothesized that a circRNA may serve as a predictor for sulindac K-80003 application in PDAC chemotherapy.

In our study, based on multi-omics data from RNA-seq, protein sequencing (Protein-seq), multiplex immunofluorescent staining (mIFS), 3D-cell in vitro models, and in vivo PDO models of AG chemotherapy-resistant PDAC (Fig. 1A), we identified the critical role of abnormal activation of the PI3K/Akt signaling pathway in chemotherapy-resistant patients. Given this characteristic, we confirmed that sulindac K-80003 can promote chemotherapy sensitivity in half of AG chemotherapy-resistant patients through a prospective internal PDAC cohort. Furthermore, these results were verified using retrospective internal and external PDAC cohort organoids. Finally, an exploration of clinical sensitization biomarkers revealed that the circular RNA cFAM124A is more sensitive and convenient for predicting sulindac K-80003 sensitization than the classic markers p-Akt (Thr308) and p-Akt (Ser473).

Results

The PI3K/Akt pathway plays a key role in AG-resistant PDAC

To elucidate which signaling pathway is closely associated with AG resistance in PDAC, we prospectively observed

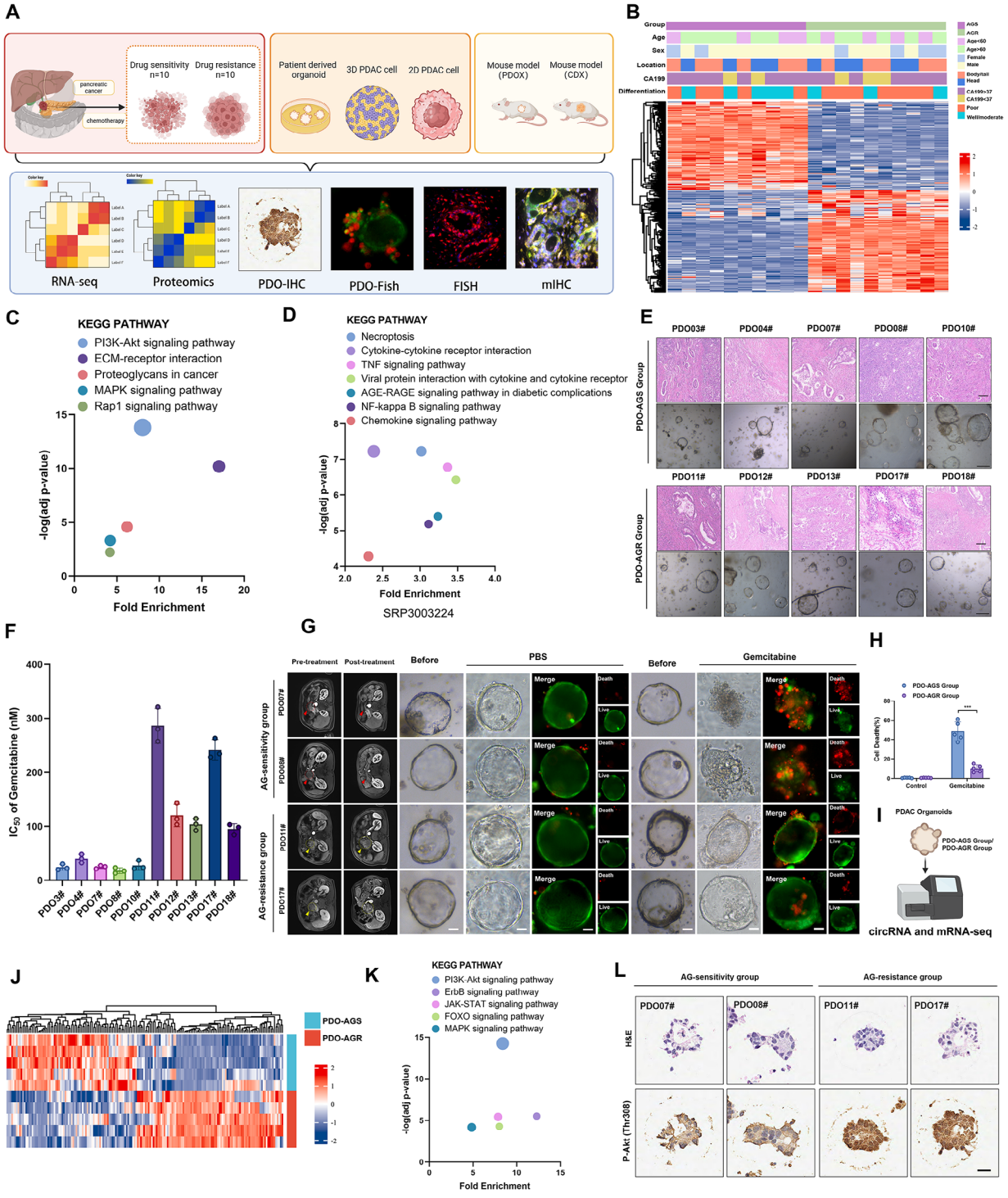

Fig. 1 PI3K/Akt pathway plays a vital role in the resistance of PDAC to GEM-based chemotherapy. **A**, Overall experimental scheme for this study. **B**, Complex heatmap showing differentially expressed genes (DEGs) and distribution of clinical parameters between AG-sensitive and AG-resistant PDAC. **C**, KEGG pathway enrichment analysis for the upregulated DEGs in the RNA-seq comparing the AG-resistant group and AG-sensitive group. **D**, KEGG pathway enrichment analysis of external RNA-seq data, SRP303224. **E**, Representative hematoxylin and eosin (H&E) staining images of AG-sensitive and AG-resistant PDAC and patient-derived organoids (PDOs). Scale bar, 100 μm. **F**, IC_{50} values for 10 PDOs after GEM treatment. G-H, Representative images of PDOs from PDO-AGS and PDO-AGR groups. PDOs treated for 48 h with nab-paclitaxel (10nM) and gemcitabine (30nM). Live/Dead cell viability staining showing live cells stained with calcein-AM (green) and dead cells with Ethidium-1 (red). Scale bar, 50 μm. **I**, RNA-seq results for PDO-AGS and PDO-AGR groups from PDOs. **J**, Heatmap showing DEGs between PDO-AGS and PDO-AGR groups. **K**, KEGG pathway enrichment analysis for upregulated DEGs in the RNA-seq comparing the PDO-AGS group and PDO-AGR groups. **L**, Representative images of H&E and IHC staining for p-Akt (Thr308) in PDOs from PDO-AGS and PDO-AGR groups

20 patients with advanced unresectable PDAC. While obtaining pathological diagnosis through biopsy, we also performed high-throughput RNA-seq and generated PDOs. These 20 patients all received AG regimen chemotherapy, and imaging and serology assessments were performed every 3 months to detect tumor changes within 6 months. We divided the patients into groups based on changes in tumor imaging (e.g., CT, MRI, and PET) [36] and CA199 expression [37].The AG-sensitive group (imaging showed that after chemotherapy, the tumor volume had shrunk or the relationship between the tumor and the surrounding blood vessels had improved, CA199 had decreased, and there were no new distant metastases, $n=10$) and the AG-resistant group (imaging showed that after chemotherapy, tumor volume was increased, the tumor invaded large blood vessels, and/or CA199 continued to increase, and/or newly-developed distant metastases appeared $n=10$) (**Table S1**). Consistently, the resistant group showed higher levels of CA199 and poorer differentiation (Fig. 1B). Kyoto Encyclopedia of Genes and Genomes (KEGG) enrichment analysis of upregulated genes in the RNA-seq comparing the AG-resistant group and AG-sensitive group showed that changes in the PI3K/Akt signaling pathway had the highest enrichment score compared with changes in other signaling pathways (Fig. 1C). In addition, the most significant difference in chemical signaling pathway changes between the external AG-resistant PDAC cohort and the non-resistant group was the PI3K/Akt signaling pathway (Fig. 1D), indicating that this signaling pathway plays a central role in PDAC chemoresistance [38]. We successfully constructed 5 AG-resistant PDO models (PDO-AGR group) and 5 AG-sensitive PDO models (PDO-AGS group) (Fig. 1E). First, we verified the drug resistance of the two groups. In vitro, the PDO-AGS group showed a lower IC_{50} and a lower percentage of dead cells under AG treatment, which also confirms the correctness of our grouping by imaging assessment (Fig. 1F-H).

We considered that the abnormal activation of the PI3K/Akt pathway observed by tissue RNA-seq previously came from derived PDAC tumor specimens representing mixed cell populations, commonly including abundant stroma cells and other cells [39]. To further clarify whether this difference exists specifically in tumor cells, we further conducted RNA-seq analysis on PDOs in the PDO-AGR and PDO-AGS groups and found that the PI3K/Akt pathway was abnormally activated in the PDO-AGR group (Fig. 1I-K). Furthermore, IHC for p-Akt (Thr308) in PDOs further supported this finding (Fig. 1L, **Fig. S1 A**). These results confirm that abnormal activation of the PI3K/Akt pathway in tumor cells plays a key role in the AG resistance of PDAC.

K-80003 enhances sensitivity to AG chemotherapy in pre-clinical models of AG-resistant unresectable PDAC cases

Given that the PI3K/AKT pathway plays a central role in the resistance of PDAC to the AG regimen, targeting this pathway in tumor cells was expected to overcome PDAC resistance to the AG regimen. However, existing PI3k/Akt inhibitors are not suitable for clinical applications due to their extensive toxicity and side effects. Therefore, we shifted our attention to the "conventional drug in new use" approach, which is also an important new strategy for developing disease treatments [25], because the safety of old drugs for use in humans has been fully proven. Our team previously focused on sulindac K-80003, a derivative of the clinical anti-inflammatory drug sulindac, as an effective PI3K/Akt pathway inhibitor. K-80003 has more reliable biological safety and superior specificity in targeting PI3K/AKT. Therefore, we explored the potential of sulindac K-80003 to overcome AG resistance in a prospectively constructed PDO-AGR group. Surprisingly, among the 5 PDOs in the AG-resistant group, sulindac K-80003 sensitized 3 PDOs (PDO11#, PDO17#, and PDO18#) to AG chemotherapy. To further analyze whether sulindac K-80003 produces similar effects in vivo, we established an orthotopic pancreatic cancer model by injecting PDOs (PDOX model). Consistent with the in vitro results, sulindac K-80003 restored sensitivity to AG significantly shrunk tumors arising and prolonged the median survival in the corresponding PDOX model (Fig. 2A-F, **Fig. S1B).** In addition, western blotting analysis further demonstrated that sulindac K-80003 could inhibit the activation of PI3k/Akt signals for patients who respond to the sensitization effect of K-80003 **(Fig. S1C)**. These important findings suggest that sulindac K-80003 is a potential drug that could enhance the sensitivity of some AG-resistant PDAC cases to AG chemotherapy.

Next, we evaluated the biosafety of sulindac K-80003 in vivo. During use, the body weight of mice in different treatment groups was similar, and the use of sulindac K80003 did not significantly change the body weight of mice. After 1 month of treatment with sulindac K-80003, the blood biochemical parameters of alanine aminotransferase (ALT), aspartate aminotransferase (AST), blood urea nitrogen (BUN), and creatinine were significantly higher than those in the saline-treated group **(Fig. S1D-S1G)**. However, no histopathological abnormalities were detected in the heart, liver, spleen, lung, or kidney of mice in the AG plus K-80003 group **(Fig. S1H-S1I)**. These results indicate that the K-80003 combined AG regimen has no significant drug toxicity in vivo and has a good safety profile.

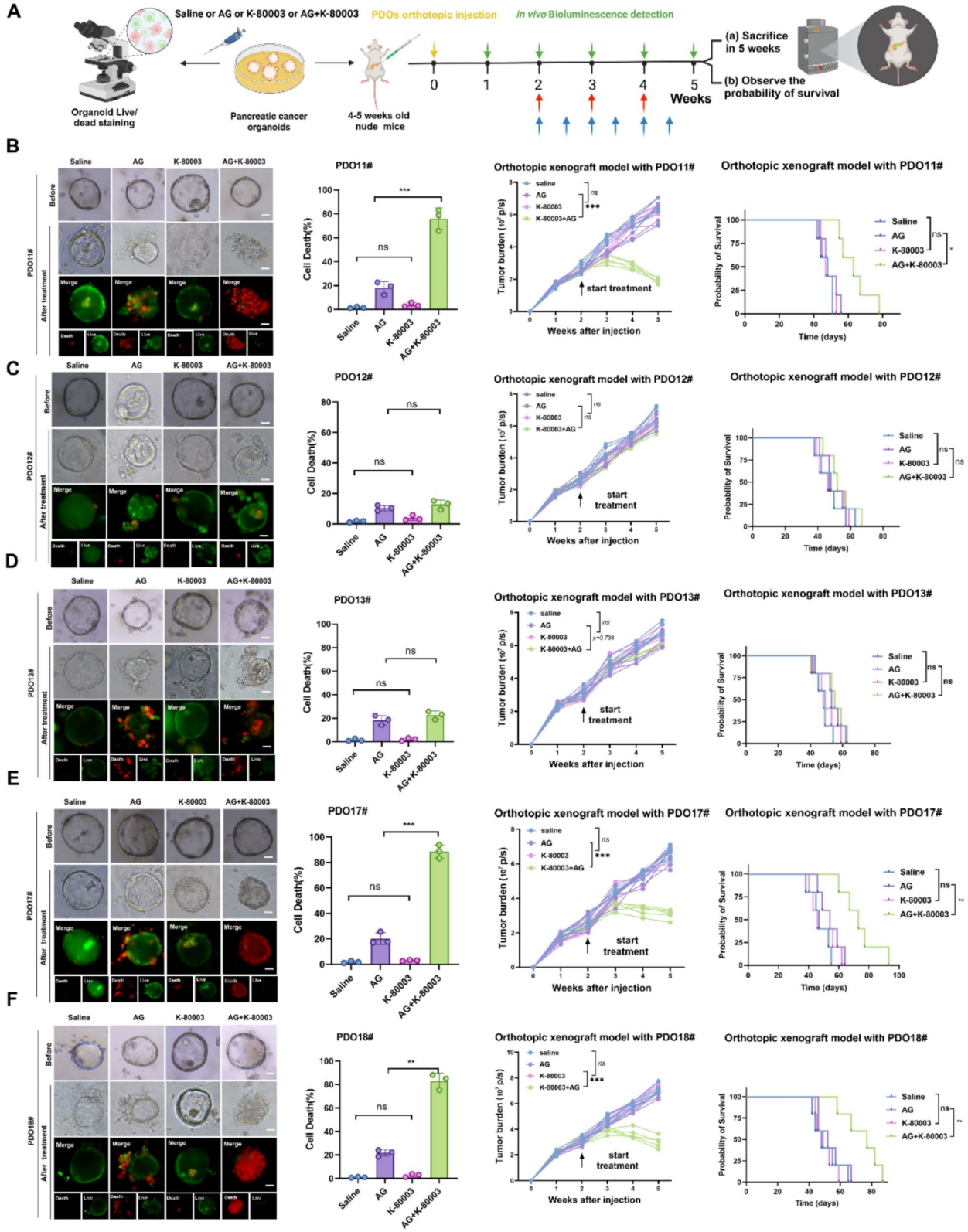

Fig. 2 (See legend on next page.)

(See figure on previous page.)

Fig. 2 K-80003 can enhance the sensitivity of some AG-resistant PDAC patients to AG chemotherapy. A, Method used to apply different treatments to PDO-AGR in vitro and quantitation of PDO fluorescence. Method used for corresponding PDOX treatments in vivo. **B-F**, Representative images of different PDO-AGRs that received different treatments. PDOs in each group treated for 48 h with saline or AG (Nab-paclitaxel 10nM plus GEM 30nM) or K-80003 (5 nM) or AG (Nab-paclitaxel 10nM plus GEM 30nM plus K-80003 5 nM). Live cells stained with calcein-AM (green), and dead cells with ethidium-1 (red). Quantitative data are shown on the right. Tumors from different groups of PDOXs received different treatments from weeks 2 after orthotopic xenograft injection of 1 million corresponding PDOs. Mice were treated with saline, K-80003 (20 mg/kg, twice weekly; bule arrows), the dual combination of gemcitabine (25 mg/kg, weekly), and nab-paclitaxel (15 mg/kg, weekly; red arrows), or the triple combination of gemcitabine and nab-paclitaxel (as dosed for the monotherapies) plus K-80003 for 3 weeks. Tumors were harvest at 3 weeks after injection. Fluorescence of tumors from mice in the different groups (5 mice per group). Survival curves for mice that received different treatments (5 mice per group). Not significant (ns), $^{*}P < 0.05$; $^{**}P < 0.01$; $^{***}P < 0.001$

K-80003 enhances sensitivity to AG chemotherapy in pre-clinical models of AG-resistant resectable PDAC cases

Considering the limited sample size of prospectively constructed advanced PDOs; to further illustrate the efficacy of sulindac K-80003 for sensitization to AG chemotherapy and to eliminate accidental errors, we conducted a retrospective study using the PDO biobank from which surgically resected tissue samples from PDAC patients are more readily available. First, we grouped patients who underwent radical surgical resection according to the international definition of drug-resistant cases after surgery for pancreatic cancer [40]. With standard GEM-based adjuvant chemotherapy after surgery, patients who developed recurrence or distant metastasis within 6 months were considered to be chemotherapy-resistant. Based on this standard, we randomly selected 12 drug-resistant PDOs from the internal biobank and randomly obtained 11 drug-resistant PDOs from the external biobank for recovery culture as shown in Fig. 3A. First, we compared the basic clinical information of the corresponding patients in the internal PDO cohort and the external PDO cohort. As shown in Fig. 3B and **Table S2**, the two cohorts showed significant differences in age, gender, and tumor stage, and the two cohorts had similar recurrence-free survival (RFS) (Fig. 3C).

Similarly, we constructed the PDOX models by injecting the PDOs, which were treated with three solutions: saline, AG, or AG plus K-80003. In the internal cohort, we found that AG combined with K-80003 treatment significantly shrunk tumors arising from 6 PDOs (PDO#II, PDO#III, PDO#VI, PDO#VIII, PDO#XI, and PDO#XII) and extended the median survival time. In contrast, the other 6 PDOs showed little response after treatment with AG combined with sulindac K-80003 (Fig. 3D-E). In the external cohort, sulindac K-80003 demonstrated the ability to sensitize 5 PDOs to AG chemotherapy (PDO#a, PDO#c, PDO#f, PDO#g, and PDO#j) (Fig. 3F-G). These results validated sulindac K-80003 as an effective AG chemosensitizing drug and promoted sensitization in half (14/28) of patients with AG-resistant PDAC in internal and external cohorts. However, considering that half of the patients still had a limited sensitization response, it is necessary to find appropriate response prediction markers to achieve patient stratification for treatment.

circRNA screening for biomarkers of the ability of K-80003 to sensitize PDAC to AG

We next used RNA-Seq analysis from PDOs to explore potential circRNA biological markers associated with the ability of sulindac K-80003 to sensitize PDAC to the AG regimen. The screening process is illustrated in Fig. 4A. First, a total of 46 differentially expressed circRNAs were identified, of which 25 were up-regulated and 21 were down-regulated (Fig. 4B). The up-regulated/down-regulated top 5 circRNAs were verified by PCR separately (Fig. 4C). Notably, this expression pattern was consistent with the PATU8988T and MiaPaCa-2 GEM-resistant models, which we constructed under continuous and progressive stimulation with GEM, and their resistance to GEM was confirmed using CCK-8 experiments and colonization experiments (Fig. 4C **and Fig. S2A-S2C**). Secondly, we defined the relative circRNA^{hi} and circRNA^{lo} in 10 cases using the median expression value as the cut-off value. Then, GSEA was performed on the read mRNA in the RNA-seq comparing the circRNA^{hi} and circRNA^{lo} groups to confirm the association between the expression of circRNA and the PI3K/AKT pathway and to calculate gene set enrichment analysis (GSEA) enrichment scores and Pearson correlation analysis (Fig. 4D and E **and Fig. S2D**). Through these studies, we identified four circRNAs as our screening indicators. Finally, we overexpressed these four circRNAs individually in PDAC cell lines to verify their drug resistance capabilities in a 3D tumor microsphere apoptosis staining assay. The experimental results show that hsa_circ_008816, hsa_circ_0030292, and hsa_circ_000620 overexpression resulted in GEM resistance, and thus, we further treated the cells expressing the GEM resistance circRNAs with additional K-80003 to examine whether their GEM-resistance could be resensitized by K-80003. We found that only overexpression of hsa_circ_0030292 (cFAM124A) had both abilities (Fig. 4F), and that cFAM124A was most closely related to activation of the PI3K/Akt pathway (Fig. 4E).

According to the circBase database, cFAM124A is formed by the circularization of exon 3 of the FAM124A

gene and is 473 nt in length. We determined the head-to-tail splicing sites of cFAM124A through Sanger sequencing **(Fig. S2E)**, and our results confirm that cFAM124A has the basic characteristics of a circRNA. cFAM124A was more resistant to RNase R degradation than the linear form of FAM124A mRNA **(Fig. S2F-S2G, Fig. S2I)**. As shown in **Fig. S2H**, cFAM124A could only be amplified from cDNA rather than gDNA, indicating that cFAM124A was a back-splicing product of the pre-mRNA. In addition, qRT-PCR and fluorescence in situ hybridization (FISH) analysis showed that cFAM124A was mainly localized in the cytoplasm, with a small amount present in the nucleus **(Fig. S2J-S2K)**.

For future research, we established PATU8988T and MiaPaCa-2 cell lines in which cFAM124A was overexpressed. PATU8988T-GR and MiaPaCa-2-GR cell lines with knockdown of cFAM124A but no change in FAM124A cellular gene expression **(Fig. S3A-S3B)**. In addition, we further examined the expression levels of cFAM124A in both the in-house cohort and external cohort PDOs (Fig. 3D and F), and the results reveals its predictive accuracy for the ability of K-80003 to sensitize PDAC to AG. We defined the cFAM124A^{hi} and cFAM124A^{lo} cases using the median expression value as the cut-off value. There were 9 cases of response among the 12 cFAM124A^{hi} PDOs (9/12) and 8 of no-response among the 11 cFAM124A^{lo} PDOs (8/11), for a true positive ratio = 75% **(Fig. S3C)**.

To further validate this finding, we investigated the activation of PI3K/Akt and expression of cFAM124A in our in-house PDAC cohort who received GEM-based chemotherapy by IHC staining and FISH. Patients were assigned to a GEM-based resistant (Gem-R) group based on RFS < 12 months. Our results showed that cFAM124A expression and activation of the PI3K/Akt pathway were robustly increased in the GEM-based resistant group (Fig. 4G). Furthermore, cFAM124A expression levels were positively correlated with activation of the PI3K/Akt pathway (Fig. 4G). cFAM124A expression was closely correlated with a higher CA199 level, poor differentiation, similar American Joint Committee on Cancer (AJCC) stage, and worse survival (Fig. 4H and **Table S3**) within the PDAC cohort in our center. Our findings suggest that only cFAM124A is associated with resistance to gemcitabine and response with K-80003, while the other four upregulated circRNAs were not associated with resistance to gemcitabine or cannot predict the response with K-80003. Also, cFAM124A is closely associated with PI3K/Akt pathway activation, and thus, we hypothesized that it may serve as a marker to identify K-80003-associated AG sensitivity in resistant PDAC.

cFAM124A is the best biomarker for the ability of K-80003 to sensitize PDAC to AG

We next focused on identifying which marker is the best marker for the ability of sulindac K-80003 to sensitize PDAC to AG chemotherapy. Sulindac K-80003 inhibits the activation of tumor-specific PI3K/Akt signaling by preventing the binding of tRXRα to the p85α subunit of PI3K [41]. Here, we further prove that this phenomenon also exists in PDAC through co-IP, as shown in **Fig. S4A**. Theoretically, sulindac K-80003 is most suitable for patients with high expression levels of tRXRα and PI3K/Akt activation markers. However, tRXRα is a truncated protein that lacks part of the N-terminal A/B domain of RXRα [41]. Due to the characteristics of its truncated protein, IHC staining analysis cannot distinguish the truncated and full-length forms, and its expression cannot be accurately calculated. Thus, it is not suitable as a predictive biomarker.

Next, we evaluated PI3K/Akt activation markers phosphorylated (p)-Akt (Thr308) and p-Akt (Ser473) as well as cFAM124A and their ability to predict response to sulindac K-80003. It is worth noting that the cFAM124A abundance differed significantly between the response group and non-response group on mIFS staining and IHC staining. (Fig. 5A and D). To further determine whether the optimal sensitive tumor markers we selected originate from tumor-specific sources rather than adjacent tissue, we used adjacent tissue as a reference to adjust the expression levels in the tumor tissue. As expected, in all samples, the expression levels of cFAM124A, p-Akt (Thr308) and p-Akt (Ser473) were higher than those in paracancer tissues (Fig. 5E and F). The fold change value for the tumor relative to the paracancer showed that cFAM124A offers good discrimination between the response group and the non-response group. On the contrary p-Akt (Thr308) and p-Akt (Ser473) showed that discrimination effects that were far inferior to that of cFAM124A, even though the *P* value for p-Akt (Sre473) reached 0.0325 (Fig. 5G and H). Interestingly, in the value selection, we found that the fold change value for cFAM124A was less than 2 for the non-responsive group, while a value greater than 2 corresponded to a responsive group. Therefore, we propose that the fold change value of 2 may be the cut-off value to distinguish groups that will be responsive and non-responsive to K-80003 (Fig. 5G-H). Based on the above analysis, cFAM124A is a practical and effective biomarker for guiding the use of sulindac K-80003 in the sensitization of PDAC to AG chemotherapy.

K-80003 reverses cFAM124A-induced GEM resistance in PDAC through the PI3K/Akt pathway

We next investigated the mechanisms underlying cFAM124A as an accurate marker for predicting the

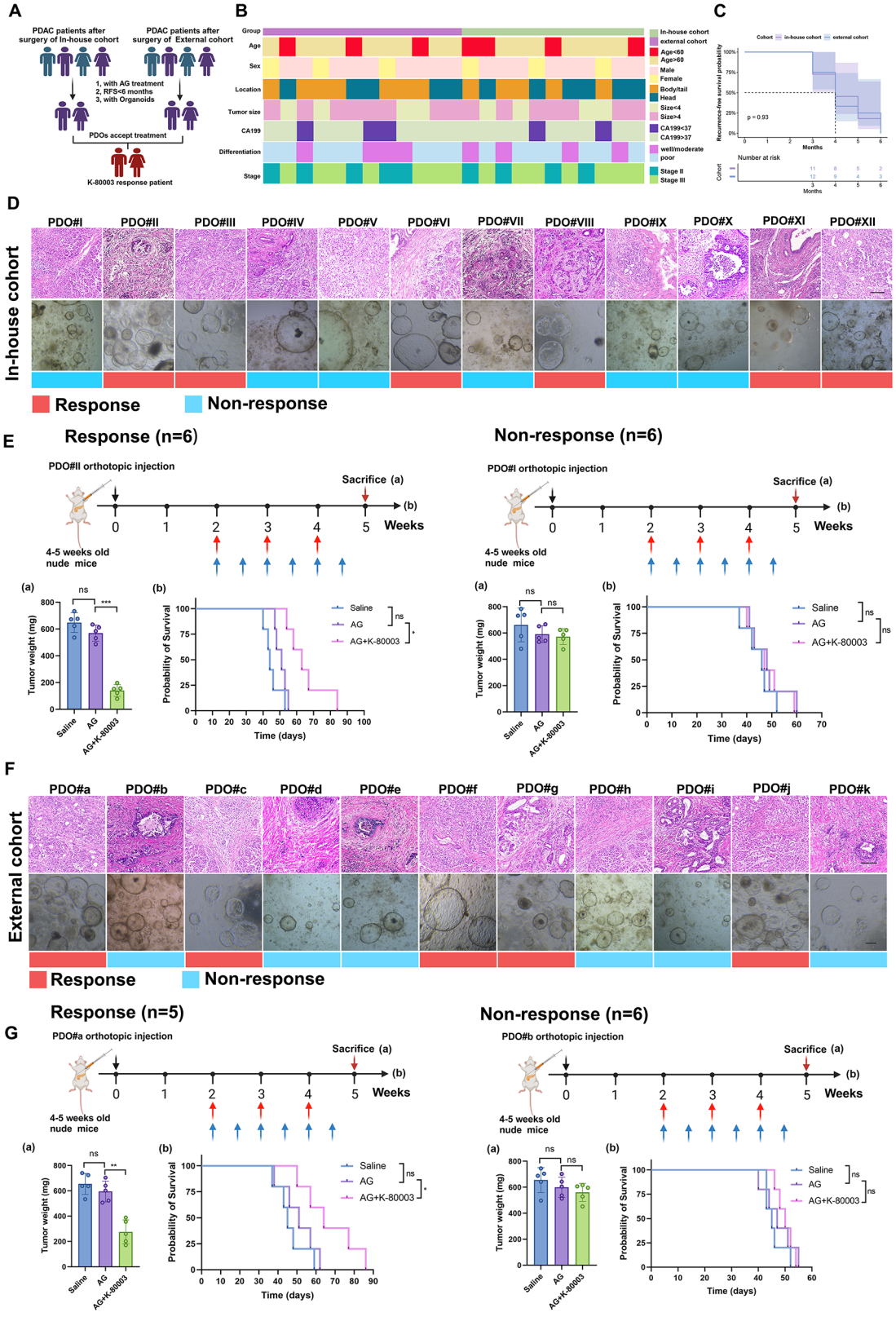

Fig. 3 (See legend on next page.)

(See figure on previous page.)

Fig. 3 Response status of AG-resistant PDAC with K-80003 treatment from in-house and external cohorts. **A**, Flow chart for screening PDAC patients for K80003 sensitization AG regimen. **B**, Complex heatmap showing distribution of clinical parameters between in-house cohort and external cohort of AG-resistant PDAC. **C**, Kaplan–Meier overall survival (PFS) curves between in-house cohort and external cohort of AG-resistant PDAC. **D**, Representative HE staining images of 12 AG-resistant PDAC samples and PODs from in-house cohort, and ability of K-80003 to sensitize samples to AG chemotherapy. **E**, Weight of tumors from mice in the different groups (5 mice per group), and survival curves for mice that received different treatments (5 mice per group). Tumors from different groups of PDOXs received different treatments from weeks 2 after orthotopic xenograft injection of 1 million corresponding PDOs. Mice were treated with saline, the dual combination of gemcitabine (25 mg/kg, weekly), and nab-paclitaxel (15 mg/kg, weekly; red arrows), or the triple combination of gemcitabine and nab-paclitaxel (as dosed for the monotherapies) plus K-80003 (20 mg/kg, twice weekly; blue arrows) for 3 weeks. Tumors were harvest at 3 weeks after treatment. Survival curves for mice that received different treatments (5 mice per group). **F**, Representative HE staining images of 11 AG-resistant PDAC-derived PDOs in external cohort, and ability of K-80003 to sensitize them to AG chemotherapy. **G**, Weight of tumors from mice in the different groups (5 mice per group), and survival curves for mice that received different treatments (5 mice per group). Not significant (ns), $^{*}P<0.05$; $^{**}P<0.01$; $^{***}P<0.001$

sulindac K-80003 drug response. Western blotting analysis further demonstrated that overexpression of cFAM124A attenuated the GEM-induced apoptosis level among PDAC cells, as indicated by cleaved caspase 3/8 levels, and promoted excessive activation of the PI3K/Akt pathway, as indicated by higher p-Akt (Thr308) and p-Akt (Ser473) (Fig. 6A). We also used a PI3K pan-inhibitor (copanlisib), which prevented aberrant activation of the PI3K/Akt pathway, and the decreased in GEM-induced apoptosis level caused by cFAM124A overexpression (Fig. 6A). Functional studies employing the CCK-8 assay, clonogenic assay, and 3D tumor microsphere apoptosis staining assay provided in vitro evidence (Fig. 6B-D) as well as in vivo evidence (Fig. 6E **and Fig. S4A)** that additional treatment with a PI3K/Akt inhibitor rescued overexpressed cFAM124A-related GEM resistance. These findings indicate that cFAM124A promotes PDAC GEM resistance by over-activating the PI3K/Akt pathway. In addition, sulindac K-80003 could also reverse the GEM resistance caused by cFAM124A. However, copanlisib caused weight loss in mice, whereas sulindac K-80003 did not (Fig. 6F), which indicates that sulindac K-80003 offers better biosafety.

CircRNAs can act by regulating protein production [42]. We performed proteomics analysis to identify changes in the expression of proteins regulating PI3K/Akt signaling upon cFAM124A overexpression. RXRα protein expression was found to be most decreased, and activation of the PI3K/Akt pathway increased after cFAM124A overexpression in PDAC cells. In contrast, cFAM124A knockdown elicited the opposite response in PDAC cells (Fig. 6G-H **and Fig. S4C)**. Interestingly, RXRα mRNA expression was not altered after cFAM124A overexpression in PDAC cells **(Fig. S4D)**. A reporter gene assay showed that cFAM124A also did not affect RXRα promoter activity **(Fig. S4E)**. This finding prompted our investigation to shift to determining the regulatory potential of cFAM124A on RXRα at the protein level. Next, we analyzed the effect of cFAM124A on the RXRα proteasome-dependent (ubiquitinated) degradation pathway [43]. cFAM124A overexpression accelerated RXRα degradation in PATU8988T cells after treatment with the protein synthesis inhibitor cycloheximide (CHX). Interestingly, this accelerated degradation of RXRα could not be abolished by the proteasome inhibitor MG132, which failed to demonstrate that the effect of cFAM124A on the RXRα degradation is proteasome-dependent (Fig. 6I-J **and Fig. S4F-S4G)**. Previous research has shown that RXRα proteins can be hydrolytically cleaved by protein hydrolases (m-calpain and CTSL) to generate truncated proteins [44, 45]. One example is tRXRα, which interacts with the p85α subunit of PI3K to activate the PI3K/Akt pathway [28]. Coincidentally, at the same time we discovered that the GEM-resistance mechanism involves aberrant activation of the PI3K/Akt pathway caused by cFAM124A overexpression, we observed increased tRXRα expression on western blotting analysis (Fig. 6H). Collectively, we found that cFAM124A activates the PI3K/Akt pathway through tRXRα, leading to GEM resistance in PDAC, and sulindac K-80003 can reverse this effect.

cFAM124A promotes tRXRα expression by upregulating the CTSL enzyme

These findings led us to hypothesize that: (1) cFAM124A may promote hydrolysis of RXRα into tRXRα, which leads to its accelerated degradation; and (2) tRXRα may be the downstream factor responsible for the cFAM124A-induced excessive activation of the PI3K/AKT pathway that leads to GEM resistance in PDAC. Thus, we investigated whether the promoted hydrolysis of RXRα leads to its accelerated degradation. Interestingly, we found that the addition of a CTSL enzyme inhibitor (Z-FY-CHO) and not an m-calpain enzyme inhibitor (PD150606) restored the decrease in RXRα and increase in tRXRα caused by cFAM124A overexpression (Fig. 7A **and Fig. S5A)**. Meanwhile, treatment with the CTSL inhibitor also restored the accelerated degradation of RXRα protein and the increase in tRXRα caused by cFAM124A (Fig. 7B **and Fig. S5B)**.

To further investigate how cFAM124A facilitates hydrolytic cleavage of RXRα in a CTSL-dependent manner, we first investigated the effect of cFAM124A on the CTSL enzyme. Our results indicated that cFAM124A

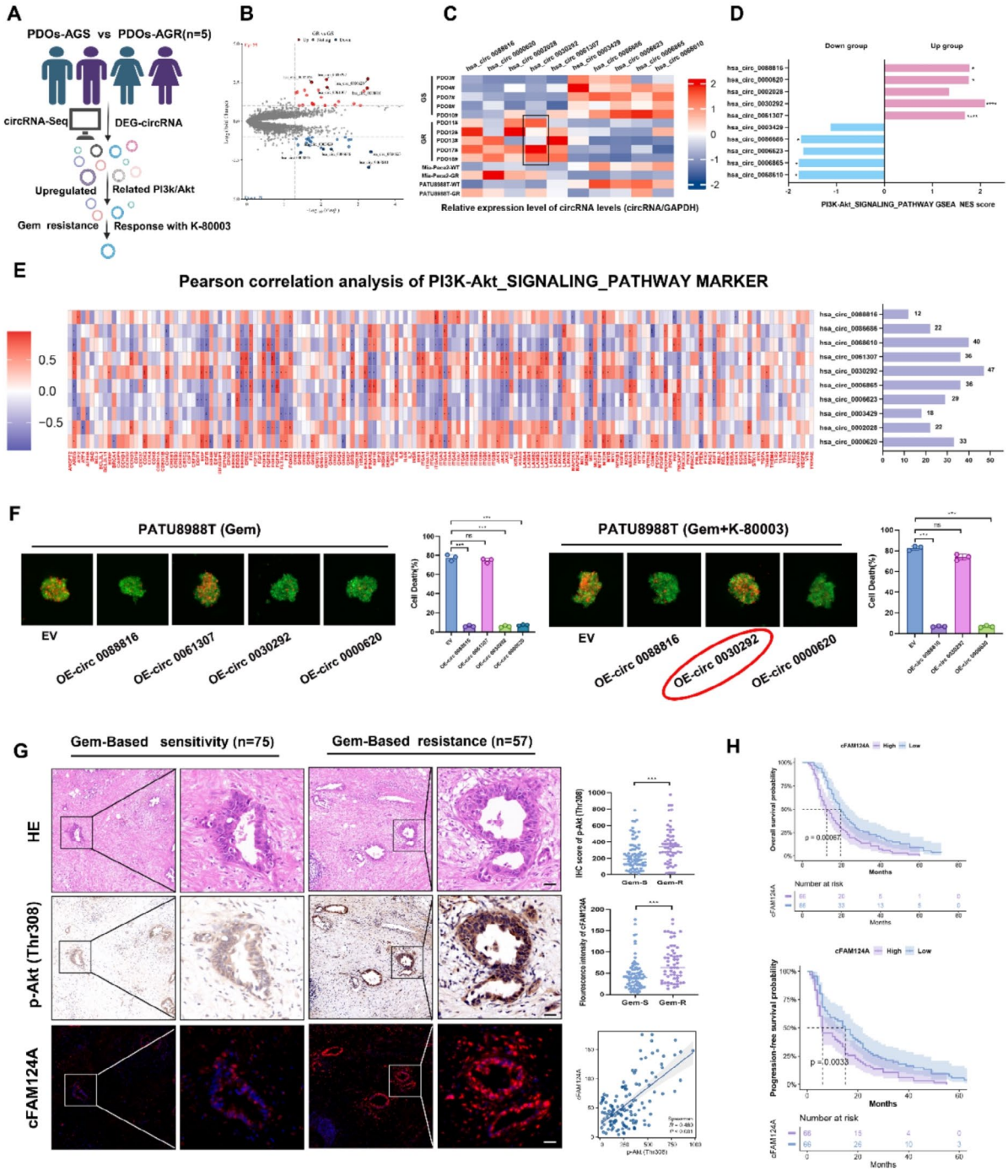

Fig. 4 cFAM124A is a potential biomarker for the ability of K-80003 to increase AG sensitivity of PDAC. **A**, Flowchart for screening for K-80003 response markers. **B**, Volcano plot showing upregulated and downregulated circRNAs between PDO-AGS and PDO-AGR groups. **C**, RT-qPCR detection of the expression of 10 relevant circRNAs in PDAC PDOs and cells. **D**, GSEA of 10 circRNAs demonstrating enrichment of DEGs in the PI3K/Akt pathway. **E**, Pearson correlation analysis between PI3K/Akt signaling pathway marker expression and the 10 circRNAs and number of related genes. **F**, Necrosis in 3D tumor microspheres based on propidium iodide (PI) staining (red) and its quantification after treatment with Gem (1 μM) and/or K-80003 (5 nM). Scale bar, 100 μm. **G**, Representative H&E and IHC staining for p-Akt (Thr308) and FISH staining for cFAM124A in samples from GEM-sensitive (Gem-S) and GEM-resistant (Gem-R) patients. Quantification of p-Akt (Thr308) staining in PDAC tissues collected from Gem-S and Gem-R groups. Quantification of cFAM124A staining in PDAC tissues collected from Gem-S and Gem-R groups. Pearson correlation analysis between p-Akt (Thr308) expression and cFAM124A expression. **H**, Kaplan–Meier OS and PFS curves according to cFAM124A expression for PDAC patients in **Table S3** ($n = 132$). Not significant (ns), $^{*}P < 0.05$; $^{**}P < 0.01$; $^{***}P < 0.001$

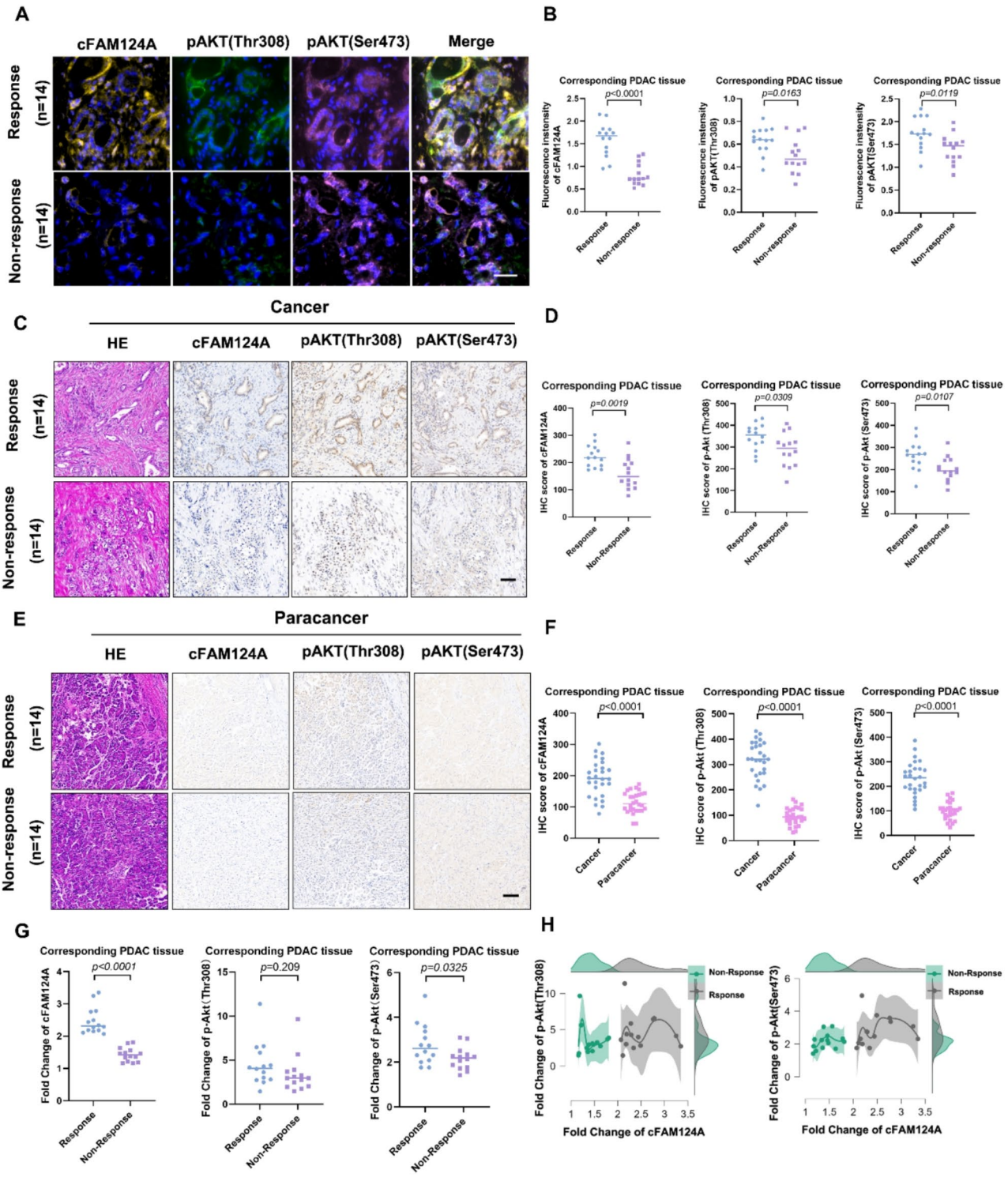

Fig. 5 (See legend on next page.)

(See figure on previous page.)

Fig. 5 cFAM124A is the best marker to predict the ability of K-80003 to promote AG sensitivity in PDAC. **A-B**, Representative multiplex IHC staining for cFAM124A, p-Akt (Thr308), and p-Akt (Ser473) expression in PDAC tissues collected from K-80003 responsive and K-80003 non-responsive groups. Quantification of cFAM124A, p-Akt (Thr308), and p-Akt (Ser473) staining in PDAC tissues collected from K-80003 responsive and K-80003 non-responsive groups. Scale bar, 100 μm. **C-D**, Representative H&E, FISH staining for cFAM124A, and IHC staining for p-Akt (Thr308) and p-Akt (Ser473) in PDAC tissues collected from K-80003 responsive and K-80003 non-responsive groups. Quantification of cFAM124A, p-Akt (Thr308), and p-Akt (Ser473) staining in PDAC tissues collected from K-80003 responsive and K-80003 non-responsive groups. Scale bar, 100 μm. **E-F**, Representative H&E, FISH staining for cFAM124A and IHC staining for p-Akt (Thr308) and p-Akt (Ser473) in paracancer tissues collected from K-80003 responsive and K-80003 non-responsive groups. Quantification of cFAM124A, p-Akt (Thr308), and p-Akt (Ser473) staining in paracancer tissues collected from K-80003 responsive and K-80003 non-responsive groups. Scale bar, 100 μm. **G**, Fold changes in cFAM124A, p-Akt (Thr308) and p-Akt (Ser473) expression levels in PDAC tissues collected from K-80003 responsive and K-80003 non-responsive groups. **H**, Peak fold changes in cFAM124A, p-Akt (Thr308), and p-Akt (Ser473) expression in different groups. Not significant (ns), $^{*}P < 0.05$; $^{**}P < 0.01$; $^{***}P < 0.001$)

promotes CTSL expression at both the mRNA and protein levels as well as CTSL activity (Fig. 7C **and Fig. S5C-S5D)**. This suggests that cFAM124A may promote the stability of CTSL mRNA, leading to an increase in the CTSL protein level. Competing endogenous RNAs (ceRNAs) often act as miRNA sponges by binding with argonaute-2 (AGO2) to regulate the stability of target mRNAs via a ceRNA-related mechanism [46]. However, we did not detect any interaction between AGO2 and cFAM124A by radioimmunoprecipitation (RIP) assay **(Fig. S5E)**, which rules out a ceRNA-related mechanism from this context. The potential ability of cFAM124A to encode proteins was not predicted by analysis of the circRNADb database **(Fig. S5F)**, which led us to investigate a protein scaffolding role of cFAM124A in regulating the stability of the CTSL mRNA.

We performed an RNA pulldown–MS assay to identify the proteins interacting with cFAM124A. AGO2 was not among the 147 proteins identified as interacting with cFAM124A. To narrow down the candidates, we considered proteins that were both identified to interact with FAM124A using MS and predicted to bind with cFAM124A using the catRAPID, RBPsuite, and RBPmap databases (Fig. 7D-E). This analysis identified insulin-like growth factor 2 RNA-binding protein 2 (IGF2BP2), which is known to stabilize mRNA [47]. Through RNA pulldown, silver staining, immunofluorescence, and RIP-qPCR assays, we confirmed the interaction between cFAM124A and IGF2BP2 (Fig. 7D-F **and Fig. S5G)**. Additionally, cFAM124A expression did not affect the abundance of IGF2BP2 **(Fig. S5H)**. Previous research showed that IGF2BP proteins preferentially bind to the "(U > C) GGAC" consensus [47]. We identified two potential IGF2BP-binding regions (namely, "CGGACU" and "UGGACA") in the cFAM124A sequence, and simultaneous mutation of both loci abolished the bridging role of the two loci that facilitates the binding of IGF2BP2 to CTSL mRNA (Fig. 7F **and Fig. S5I-S5J)**. In addition, siRNA-mediated silencing of IGF2BP2 led to accelerated degradation of CTSL mRNA and protein levels in vitro **(Fig. S5K-S5M)**.

Next, we identified a potential m6A site on the 3′-untranslated region (UTR) of the CTSL mRNA **(Fig. S4N)**, and then we confirmed the interaction between IGF2BP2 and CTSL mRNA by RNA pulldown assay (Fig. 7G). In addition, RNA antisense purification (RAP) assay using the cFAM124A probe also enriched CTSL mRNA (Fig. 7H). Based on this evidence of the interactions among cFAM124A, CTSL mRNA, and IGF2BP2, we propose a potential regulatory mechanism by which cFAM124A promotes the stability of CTSL mRNA. As expected, cFAM124A overexpression increased the interaction between IGF2BP2 and CTSL mRNA, leading to slower degradation of CTSL mRNA (Fig. 7I**).**

We further constructed a truncated form of IGF2BP2 to examine IGF2BP2-mediated stabilization of the direct functional domain of CTSL mRNA (the functional threshold for recognition of m6A, known as KH4) and the cFAM124A-dependent indirect facilitation of the functional threshold (the functional threshold for binding by cFAM124A, known as KH1) (Fig. 7J). These results validate our hypothesis that cFAM124A binds to IGF2BP2 to stabilize CTSL mRNA in an m6A-dependent manner, thus playing a bridging role (Fig. 7K).

Notably, mutation of the scaffold site on cFAM124A completely reversed the cFAM124A overexpression-induced increase in CTSL expression at both the mRNA and protein levels (Fig. 7L-M). However, it could only partially reverse the increased CTSL activity, increased tRXRα level, aberrant activation of the PI3K/Akt pathway, and increased GEM resistance caused by cFAM124A overexpression (Fig. 7M-N). Interestingly, the entirely reversed effects on the tRXRα/PI3K/ATK pathway and GEM resistance by small interfering (si)-CTSL treatment suggested that the promoting effect of cFAM124A for PDAC GEM resistance depends not only on its effect on CTSL expression but also on its other effects on CTSL activity (Fig. 7M-N). The present findings indicate that cFAM124A upregulates CTSL mRNA and protein expression through bridging, and cFAM124A also affects CTSL enzyme activity through other mechanisms.

cFAM124A enhances CTSL enzyme activity by disrupting cystatin B (CSTB)

The activity of CTSL is mainly regulated by the endogenous cystatin superfamily members, particularly by stefin A (cystatin A, CSTA) and stefin B (cystatin B, CSTB) [48], which inhibit CTSL activity by binding to the C-terminal of CTSL. cFAM124A overexpression did not affect CSTA or CSTB protein expression **(Fig. S6A)**. We reviewed the cFAM124A-interacting proteins identified through the RNA pulldown–MS assay and observed interactions between cFAM124A and CSTB (Fig. 7E **and** Fig. 8A). In addition, their interaction was confirmed in the catRAPID database and confirmed through immunofluorescence, RIP, and RNA pulldown assays (Fig. 8B-C **and Fig. S5B)**. Interestingly, cFAM124A overexpression in PATU8988T significantly weakened the CTSL–CSTB interaction. In contrast, the interaction between CTSL and CSTB was strengthened upon cFAM124A knockdown (Fig. 8D-E). This suggests that cFAM124A can interact with CSTB protein to interfere with the binding of CSTB to CTSL, thus enhancing CTSL enzyme activity.

To further characterize how cFAM124A interacts at this competitive site, we predicted the competitive site of cFAM124A that binds to CSTB using the catRAPID database and constructed cFAM124A plasmids with truncated corresponding regions for transfection of PATU8988T cells (Fig. 8F). RNA pulldown and coimmunoprecipitation (co-IP) assays showed that when the 76–210-nt region of cFAM124A was truncated, CSTB protein capture by the circRNA probe was significantly reduced, correlating with increased binding of CSTB to CTSL (Fig. 8G-H). In addition, mutation of the competitive site also attenuated, but not entirely abolished, the increase in tRXRα, aberrant elevation of PI3K/Akt pathway activation, and GEM resistance caused by cFAM124A overexpression, as reflected by results from western blotting analysis, CTSL enzyme activity detection, 3D tumor microsphere staining, and colony formation assay (Fig. 8I-J **and Fig. S6C-D)**. Interestingly, these effects were reversed by simultaneous mutation of the cFAM124A bridge site and the competitive site, (Fig. 8I-J **and Fig. S6D-S6E)**. Together these results suggest that cFAM124A upregulates CTSL expression through IGF2BP2 and by interfering with the inhibition of CTSL enzyme activity by binding to CSTB. In turn, this leads to excessive hydrolytic cleavage of RXRα by CTSL and generates tRXRα which excessively activates the PI3K/Akt pathway and promotes GEM resistance in PDAC.

Discussion

The AG regimen is well tolerated and the first choice for the treatment of advanced PDAC in Asia. However, most patients develop chemotherapy resistance, resulting in poor prognosis. Unlike previous studies, which focused on the exploration of drug resistance mechanisms in pancreatic cancer and the prediction of sensitivity markers, we focused on exploring new treatment strategies for sensitization of PDAC to AG regimens. Considering the clinical limitations of immunotherapy combination regimens, we focused on combination strategies with tumor pathway inhibitors. We used the PDO model and RNA-seq of samples from patients with advanced pancreatic cancer to accurately distinguish the drug-resistant group and drug-sensitive group according to the clinical effects of AG treatment. We confirmed that activation of the PI3K/Akt pathway plays a central role in drug resistance in pancreatic cancer [12]. In addition, we adopted the strategy of "conventional drug in new use" that offers great health and economic benefits and selected the established drug sulindac K-80003, a sulindac-derivative, that inhibits PI3K/Akt. We first confirmed its effectiveness without surgery through five prospectively collected PDO models from drug-resistant patients. We also confirmed K-80003 clinical potential in randomly screened and established PDO models of postoperative drug-resistant patients in internal and external cohorts to expand the sample size. Our results demonstrated that K-80003 could sensitize nearly half of the models. In addition, to identify the population for which sulindac K-80003 was effective, we discovered that cFAM124A is the most sensitive and convenient sensitization biomarker, as it was not only more sensitive than the traditional PI3K/Akt activation markers but also associated with the effect target of K-80003, tRXRα. Thus, our research provides a new practical treatment strategy for the clinical sensitization of PDAC to AG chemotherapy.

Abnormal activation of the PI3K/Akt pathway is closely related to the occurrence and progression of PDAC. We established the PDO model using biopsy specimens of unresected advanced pancreatic cancer. We believe that the results from actual tumor-bearing patients can more accurately reflect the sensitivity and resistance tendencies to the AG regimen. Although it was difficult to construct PDOs from biopsy specimens, we still successfully constructed half of the models. We examined changes in mainstream cancer signaling pathways and identified the central role of the PI3K/Akt pathway in chemotherapy resistance, consistent with previous literature [12, 13]. Activation of the PI3K/Akt pathway could promote chemotherapy resistance in various ways, such as regulating the expression of P-gp and ABC transporters to enhance drug efflux [49–51]. These results reveal the clinical potential of interfering with the PI3K/Akt pathway to achieve chemotherapy sensitization. However, the PI3K/Akt pathway is also critical for normal physiological function [52], and thus, clinical use of PI3K/AKT pathway inhibitors (such as Everolimus) can lead to many clinical adverse reactions [22, 23]. Therefore, we focused

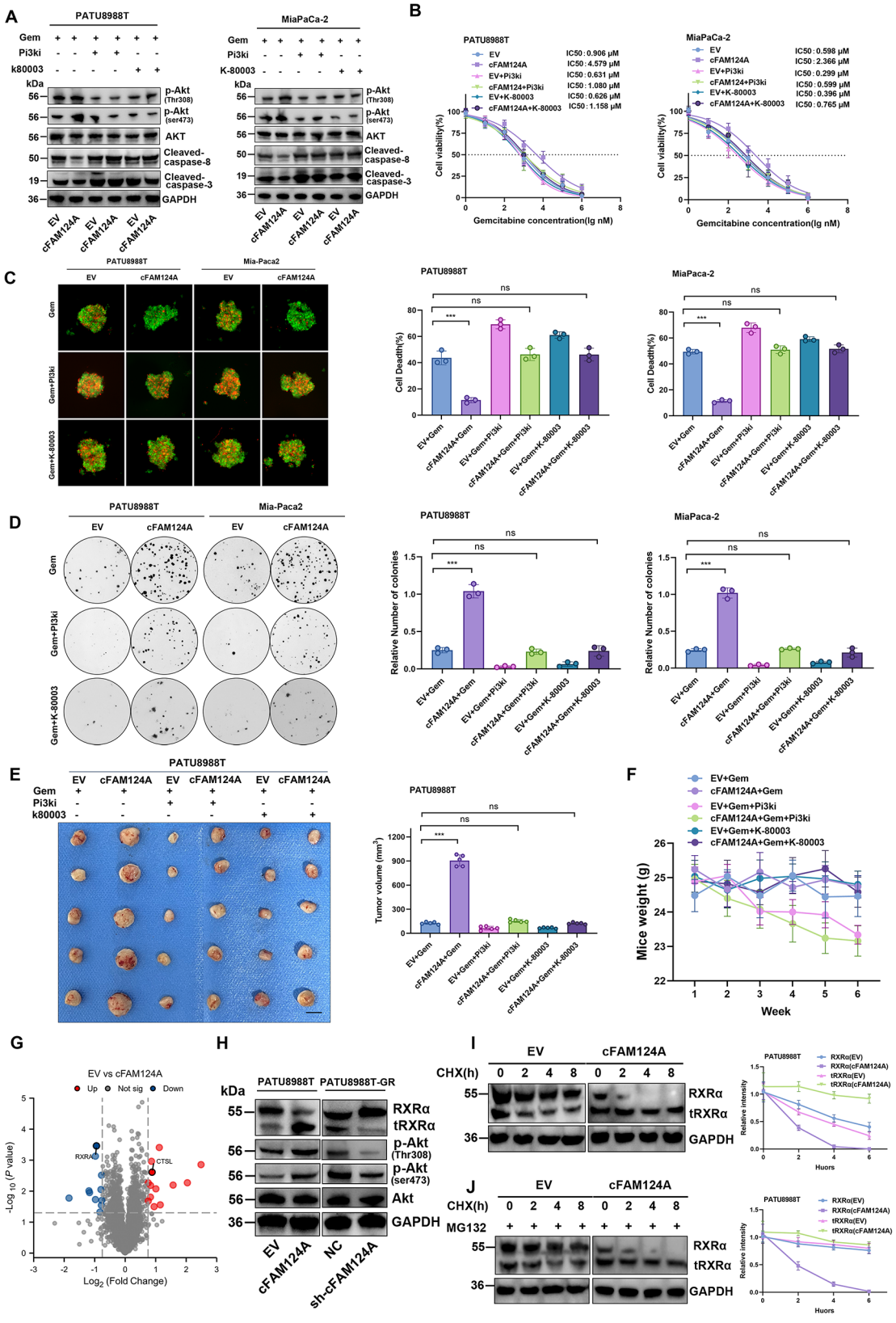

Fig. 6 (See legend on next page.)

(See figure on previous page.)

Fig. 6 cFAM124A activates PI3K/Akt pathway through tRXRα to cause GEM resistance in PDAC, and K-80003 can reverse this effect. **A**, Western blot analysis of Akt, p-Akt (Ser473), p-Akt (Thr308), and cleaved caspase 3/8 expression after 6 h of treatment with different inhibitors and GEM treatment. **B**, IC_{50} values for GEM in PDAC cells overexpressing cFAM124A and control cells after 6 h of treatment with different inhibitors and GEM treatment. **C**, Necrosis in 3D tumor microspheres based on PI staining (red) and after 6 h of treatment with different inhibitors and GEM treatment. Scale bar, 100 μm. **D**, Colony formation by cells overexpressing cFAM124A after 6 h of treatment with different inhibitors and GEM treatment in 6-well dishes (800 cells/well) for 2 weeks. Each inhibitor, copanlisib (2 nM, pan-PI3K inhibitor) or K-80003 (5 nM, tRXRα-dependent Akt activation inhibitor). Quantitative data are shown on the right. **E**, Subcutaneous xenograft model of mice in the different groups treated with GEM (40 mg/kg i.p. 2×/week for 4 weeks), copanlisib (1 mg/kg, iv. 2×/week for 4 weeks), or K-80003 (20 mg/ kg i.p. 2×/week for 4 weeks) at 2 weeks after subcutaneous injection of 5×10^6 cells overexpressing cFAM124A and control cells. Representative images of tumors are shown ($n = 5$). **F**, Body weights of subcutaneous tumor-bearing mice in the indicated groups ($n = 5$). **G**, Volcano plot showing upregulated and downregulated protein between EV-PATU8988T and cFAM124A-PATU8988T cells. **H**, Western blot analysis of RXRα, Akt, p-Akt (Ser473), and p-Akt (Thr308) expression in PDAC cells overexpressing cFAM124A or with cFAM124A knockout and control cells. **I**, cFAM124A increased RXRα protein degradation: Indicated PDAC cell lines were incubated with CHX for indicated time periods before western blot analysis of RXRα and GAPDH expression. Representative images are shown (left). **J**, Indicated PDAC cell lines were incubated with MG132 and then with CHX for indicated time periods before western blot analysis of RXRα and GAPDH expression. Representative images are shown (left)

on the clinical strategy of repurposing old drugs. Since sulindac K-80003 inhibits PI3K/Akt, we first confirmed that sulindac K-80,003 can promote sensitization to AG in the PDO model from biopsy specimens (3/5). We further expanded the sample size and randomly selected 12 drug-resistant models from the PDO model library of surgical patient specimens in our center and established an external validation cohort of 11 cases. We then found nearly half (11/23) were resistant to AG from the in vivo layer, and the drug-resistant PDO model could achieve chemotherapy sensitization. Based on half of the total sample showing benefit (14/28), we believe that sulindac K-80003 is a potential AG chemotherapy-sensitizing drug for pancreatic cancer. Based on its good safety, we plan to conduct clinical research on suitable patients in the future. However, considering that half of the patients still had a limited sensitization response, it is important to find additional response prediction markers to achieve patient stratification for treatment.

Sulindac K-80003 inhibits the activation of tumor-specific PI3K/Akt signaling by preventing the binding of tRXRα to the p85α subunit of PI3K. Theoretically, sulindac K-80003 is most suitable for patients with high expression of tRXRα and PI3k/Akt signaling markers. We also investigated the possibility of using tRXRα as a marker. However, tRXRα, as a truncated protein of RXRα protein, does not have specific antibodies and is difficult to detect directly through conventional RNA-seq or proteomic sequencing. It is also difficult to distinguish tRXRα from RXRα by IHC, which makes the use of tRXRα as a predictive marker unfeasible.

circRNAs have become one of the first choices for drug treatment markers due to their stable structure, long half-life, and convenient detection methods [30, 31]. Therefore, we explored circRNAs as potential biological markers for sensitizing properties. In prospective samples, we screened and eliminated markers that were consistent with high expression of AG-resistant PDO and were related to the PI3K/Akt pathway. We discovered that cFAM124A represent a potential marker reflecting sensitization by sulindac K-80003. We further verified its reliability by combining internal and external data and found that patients with high expression can achieve chemotherapy sensitization. In addition, we found that cFAM124A is generally more effective than p-Akt (Thr308) and p-Akt (Ser473). In previous studies, only the difference between cancer tissue and adjacent tissue was considered, and the impact of adjacent tissue on cancer was ignored [53]. However, this is very important in practical applications. Therefore, we further used paracancer tissue for correction and applied the fold change value for tumor tissue compared with paracancer tissue to predict whether sulindac K-80003 would be effective. The fold change value for cFAM124A showed good discrimination between the response group and the non-response group. However, p-Akt (Thr308) and p-Akt (Ser473) failed to distinguish the groups, which further demonstrates that cFAM124A is a better marker of true tumor characteristics. Interestingly, a fold change value 2 was used as the cut-off value to distinguish the response to sulindac K-80003. Therefore, we believe that cFAM124A is a reliable and practical biomarker for predicting sensitization to AG chemotherapy in clinical practice. The predictive efficacy of the cut-off value of 2 requires further technical development in real-world clinical studies with large sample sizes.

We next investigated molecular mechanisms underlying cFAM124A effects. We found that overexpression of cFAM124A resulted in a significant decrease in RXRα protein levels. Additional studies using CHX and MG132 inhibition experiments ruled out factors affecting the production and degradation of RXRα protein. Interestingly, we found that RXRα truncated form, tRXRα, was significantly increased. We demonstrated that cFAM124A promoted CTSL (a major member of the cysteine protease family, the main proteolytic enzyme that hydrolyzes RXRα to tRXRα) [45] mRNA expression, protein expression, and enzyme activity. circRNAs often exert biological functions by binding to RNA-binding proteins [54]. We demonstrated that cFAM124A binds to IGF2BP2 protein (which functions to stabilize mRNA) and verified that it can bind to the CTSL mRNA 3′-UTR,

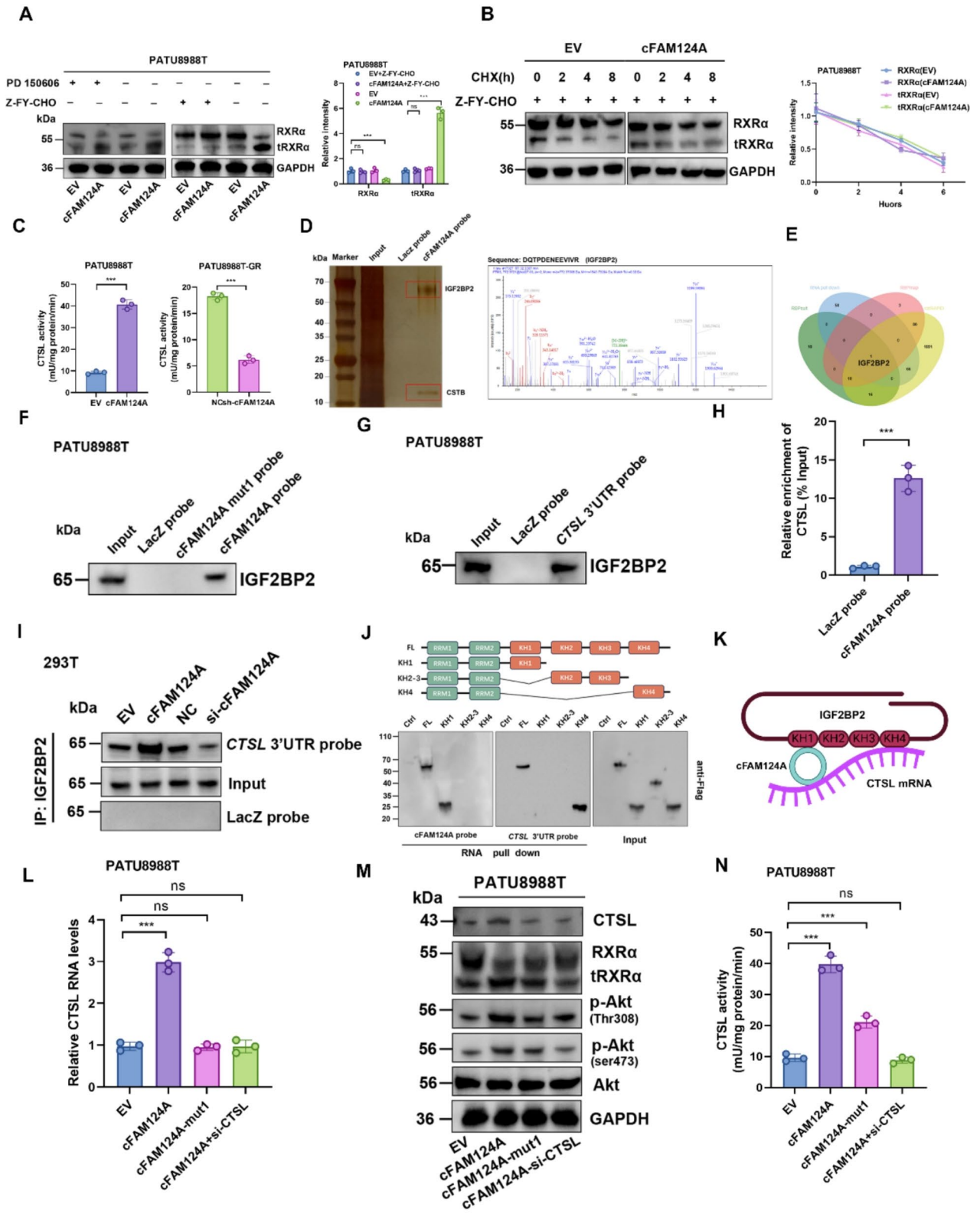

Fig. 7 (See legend on next page.)

(See figure on previous page.)

Fig. 7 cFAM124A upregulates CTSL enzyme expression through bridging effect and promotes an increase in the tRXRα protein level. **A**, Western blot analysis of RXRα expression after 24 h of treatment with PD150606 (200 nM, m-calpain inhibitor) or ZFY-CHO (10 μM, CTSL inhibitor). Representative images are shown (left). **B**, Indicated PDAC cell lines were incubated with ZFY-CHO and then with CHX for indicated time periods before western blot analysis of RXRα and GAPDH expression. Representative images are shown (left). **C**, CTSL enzyme-linked immunosorbent assay (ELISA) in PDAC cells with cFAM124A overexpression or knockout. **D**, Potential cFAM120A-binding proteins were pulled down in cell lysate by RAP assay; these were incubated with the cFAM124A probe and subsequently visualized by MS and silver staining. **E**, Venn diagram showing the overlap of potential binding proteins of cFAM124A. **F**, IGF2BP2 was pulled down by the LacZ probe (control) or cFAM124A probe and cFAM124A mutant. **G**, IGF2BP2 was pulled down by the CTSL 3′-UTR probe after overexpression of CTSL 3′-UTR. **H**, Association of cFAM124A with CTSL mRNA on RAP assay. **I**, IGF2BP2 was pulled down by the CTSL 3′-UTR probe on western blotting in the indicated groups. **J**, Upper: Schematic of the RNA-binding domain within IGF2BP2 and list of different IGF2BP2 truncation mutants. Lower: Immunoblotting with anti-Flag antibody after RNA pulldown assay in PATU8988T cells using RNA cFAM124A or CTSL mRNA probes. **K**, Pattern diagram of binding among cFAM124A, CTSL mRNA, and IGF2BP2. **L**, CTSL mRNA expression in the indicated groups. **M**, CTSL, Akt, RXRα, p-Akt (Thr308), and p-Akt (Ser473) protein expression in the indicated groups. **N**, CTSL protein concentrations detected by ELISA in the indicated groups

helping CTSL mRNA and IGF2BP2 protein to form a more stable complex. This was consistent with the fact that most circRNAs exert the function of stabilizing mRNA [55, 56]. Interestingly, we found that interfering only with its binding site could only partially restore the activity of CTSL protease. This led us to speculate that cFAM124A can also affect the enzymatic activity of CTSL through other mechanisms.

Further analysis of the proteins bound by cFAM124A revealed that cFAM124A could also bind to CSTB protein. CSTB is an endogenous inhibitor of the cysteine protease and can negatively regulate the activity of CTSL protease [48]. Using co-IP experiments, we found that cFAM124A sequesters the CSTB protein and interferes with its ability to bind to CTSL, resulting in enhanced CTSL enzyme activity. When interfering with the binding sites of cFAM124A, IGF2BP2, and CSTB at the same time, the expression of tRXRα protein and the abnormal activation state of PI3K/Akt could be restored, which was also consistent with the drug resistance functional phenotype. In summary, our results showed for the first time that some AG-resistant PDAC patients can benefit from K-80003, which improves their sensitivity to AG regimens. This may be due to the high expression of cFAM124A in these cases. High expression of cFAM124A affects the expression and activity of the CTSL enzyme. RXRα is hydrolyzed by CTSL protease into tRXRα, which enhances AKT phosphorylation through interaction with the PI3K subunit p85α and the development of AG resistance. K-80003 directly acts as a site to intervene in the interaction between tRXRα and p85α, inhibit activation of the PI3K/Akt signaling pathway, and weaken AG resistance.

cFAM124A affects the mRNA expression and enzyme activity of CTSL through two mechanisms. We also observed a high positive correlation between the expression levels of cFAM124A and tRXRα, which makes cFAM124A a substitute for tRXRα to guide the use of sulindac K-80003.

This study has certain limitations. We used a prospective PDO model to construct biopsy specimens from patients with advanced pancreatic cancer. Due to the small amount of biopsy samples, the sample size for this part of the study was limited. We prospectively evaluated patients with unresectable advanced stages treated with the AG regimen to define drug resistance. This type of sample is extremely representative. Moreover, we also used PDOs randomly obtained from the retrospective sample library (the sample size was 4 times that of the prospective sample), and the results also confirmed the finding that sulindac K-80003 has the therapeutic potential to overcome AG resistance. The sample library also provides a current sample, and this was one of the largest PDO-based studies of pancreatic cancer. In addition, according to our results, CTSL protease may be used as another potential biomarker of response to sulindac K-80003. However, due to the instability of the protease, its short half-life, its enzymatic activity subject to interference from temperature, and physical and chemical properties, making its in vitro detection difficult. Therefore, we believe that cFAM124A is the optimal biomarker for predicting the ability of K-80003 to overcome AG resistance in PDAC.

Conclusion

The new use of an old drug in combination with chemotherapy offers a safe and effective new strategy to solve the problem of drug resistance in PDAC. The results of this study show that sulindac K-80003, is a safe and effective old drug, that can enhance the sensitivity of pancreatic cancer to AG chemotherapy. This new use of K-80003 provides a new treatment option for clinical use. In addition, we report that cFAM124A is a biological marker that predicts the sensitization effect of sulindac K-80003 in patients with PDAC.

Methods

Human PDAC specimens

Human PDAC tissues from Fujian Provincial Hospital, Fujian Medical University Union Hospital and the First Affiliated Hospital of Fujian Medical University were used for IHC, generation of PDOs, RNA-seq and mIHC. Shanghai Outdo Biotech Co., Ltd provided the technical support for mIHC. This study was approved

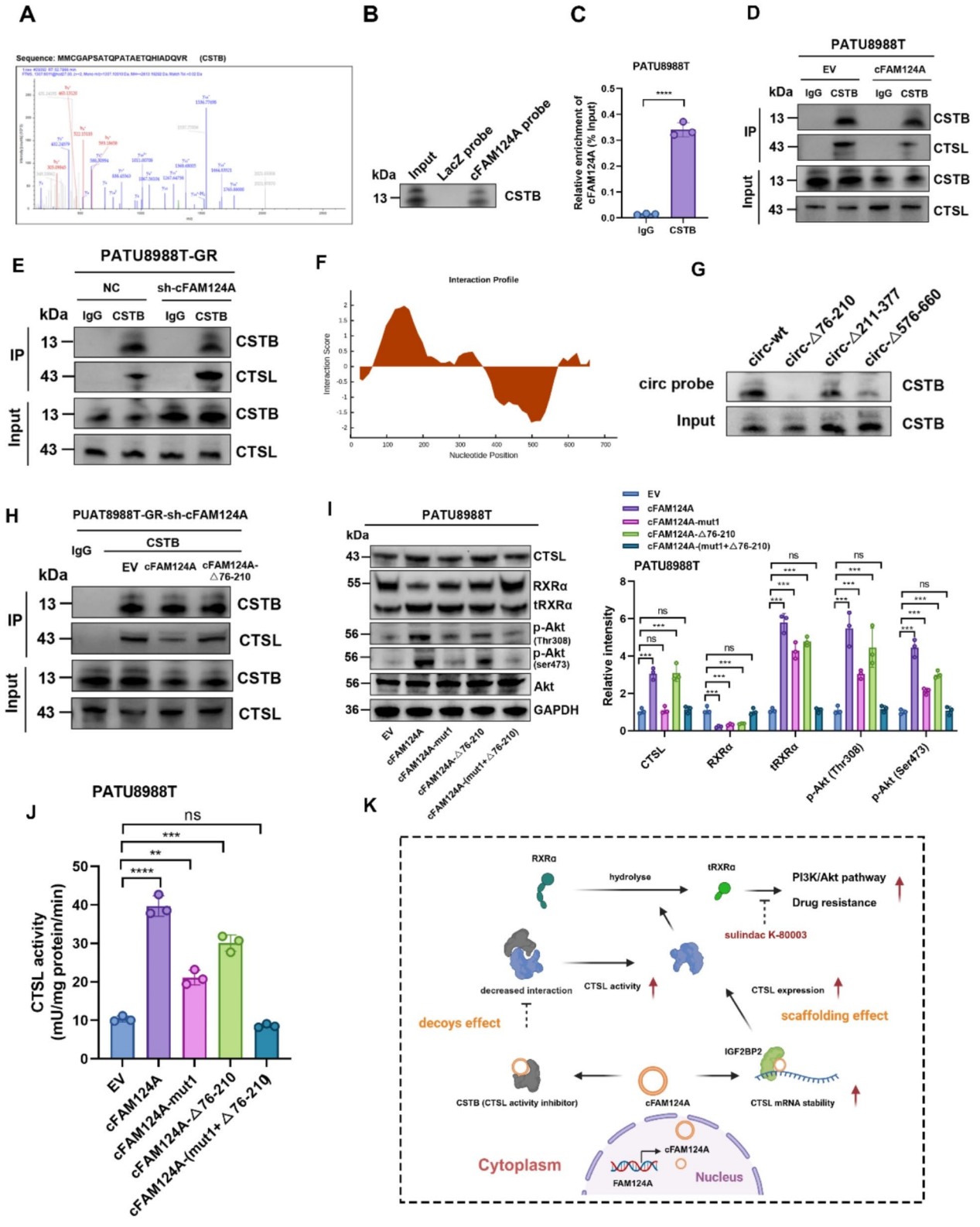

Fig. 8 (See legend on next page.)

(See figure on previous page.)

Fig. 8 cFAM124A competes with CSTB through bait effect and enhances CTSL enzyme activity. **A**, MS of CSTB protein. **B**, CSTB was pulled down by the cFAM124A probe or LacZ probe (control). **C**, RIP assay showing the association of CSTB with cFAM124A. **D-E**, Co-IP assay of CSTB and CTSL in PDAC cells with cFAM124A overexpression or knockout. **F**, Predicted binding regions in cFAM124A for CSTB by CatRAPID. **G**, After PATU8988T cells were transfected with plasmids for wild-type or truncated cFAM124A overexpression, RNA pulldown assay was performed with cFAM124A-specific probes. **H**, Co-IP assay of CSTB and CTSL in PDAC cells in different treatment groups. **I**, Western blot analysis of CTSL, RXRα, Akt, p-Akt (Ser473), and p-Akt (Thr308) protein expression in the indicated groups. **J**, CTSL concentrations by ELISA in the indicated groups. **K**, Proposed mechanism by which cFAM124A promotes PDAC chemoresistance via "scaffolding" and "decoys-like" effects. Not significant (ns), $^{*}P < 0.05$; $^{**}P < 0.01$; $^{***}P < 0.001$

by the Ethics Committee of Fujian Provincial Hospital (Fuzhou, China).

Cell lines

The PATU8988T and Mia-Paca2 human PDAC cell lines were obtained from the American Type Culture Collection (ATCC, Manassas, VA, USA). The cells were cultured in ATCC-recommended standard media supplemented with heat-inactivated fetal bovine serum (FBS) and antibiotics (50U/mL penicillin and 50 mg/L streptomycin) in a humidified atmosphere at 37℃ containing 5% CO_2. The GEM-resistant cell lines PATU8988TGR and MiaPaCa-2-GR were generated by treatment with intermittently increasing drug concentrations. The half-maximal inhibitory concentration (IC50) values for the resistant cell lines were detected, and the resistance index (RI) was calculated as follows: RI of the resistant cell line=IC50/IC50 of the parental cell line. An RI>5 indicated a resistant strain. All cell lines were tested to confirm that they were free of mycoplasma and authenticated by short-tandem repeat analysis.

Cell transfection

Hsa_circ_0030292 (cFAM124A) lentiviruses or plasmids were purchased from HANBIO (Shanghai, China). Lentivirus transfection was performed by Genechem (Shanghai, China) and plasmids were transfected into cells using the Roche Transfection Reagent (Roche, Basel, Switzerland).

Culture of pancreatic cancer patient-derived organoids (PDOs)

PDOs were generated from PDAC tissue harvested from cancer patients with GEM-sensitive or GEM-resistant PDAC. First, the tumor tissues were washed with phosphate-buffered saline (PBS) and cut into small pieces (2–3 mm3) with sterile surgical scissors. Second, the tissue samples were digested in MasterAim™ Tissue Enzyme Solution I (AIMINGMED, 100−051) in Advanced Dulbecco's Modified Eagle Medium (DMEM)/F12 medium (Thermo Fisher Scientific) for 1 h at 37 °C with intermittent shaking. Third, an additional Digestion™ Tissue Enzyme Solution I (AIMINGMED, 100−051) from MasterAim was applied. From the collected cell samples, aliquots of 600 cells resuspended in 30 μL Matrigel (356231, Corning, NY, USA) were added to individual wells of a 48-well plate and incubated at 37 °C for 5 min to allow solidification of the Matrigel. Cells were cultured in alkaline medium (advanced DMEM/F12, 10 mM HEPES, 1× GlutaMAX-I, 100 μg/mL Primocin, and 1× penicillin/streptomycin solution) or complete medium (advanced DMEM/F12, 10 mM HEPES, 1×GlutaMAX-I, 100 μg/mL Primocin, 1× penicillin/streptomycin solution, 500 nM A83-01, 10 μM Y-27632, 1.56 M N-acetylcysteine, 10 mM nicotinamide, 10 ng/mL fibroblast growth factor 10 [FGF10], 1× B27 supplement, 10 μM forskolin, 30% Wnt3A conditioned medium, 2% R-corresponding conditioned medium and 4% Noggin conditioned medium). The medium was changed every 3 days.

Live/dead staining of PDOs

PDOs were treated for 48 h with saline or AG (Nab-paclitaxel 10nM plus GEM 30nM) or K-80003 (5 nM) or AG (Nab-paclitaxel 10nM plus GEM 30nM plus K-80003 5 nM) before staining with a Live (calcein-AM)/Dead (NucRed D) staining kit (BestBio, Shanghai, China), and images were obtained using an inverted fluorescence microscope.

RNA isolation and reverse transcription-quantitative polymerase chain reaction (RT-qPCR)

Total RNA was extracted using the TRIzol reagent (Thermo Fisher Scientific, USA), and RT was performed using the PrimeScript RT Reagent Kit (Takara, Shanghai, China). Real-time PCR analyses were performed using the StepOnePlus™ Real-Time PCR System (Thermo Fisher Scientific, USA). Relative mRNA/circRNA expression levels were normalized to glyceraldehyde- 3-phosphate dehydrogenase (GAPDH) expression using the 2-ΔΔCT method.

Ribonuclease R (RNase R) treatment and actinomycin D assay

For the RNase R digestion assay, total RNA from PATU8988T and MiaPaCa-2 cells was treated with or without 5 U/μg RNase R (RNR07250, Epicenter Technologies) and incubated at 37 °C for 30 min. For the actinomycin D assay, cells were treated with 2 μg/mL actinomycin D (Sigma, USA) for 0, 4, 8, 12, or 16 h. RT-qPCR analysis was performed to detect the expression levels of cFAM124A and FAM124A. Experiments were performed three times.

Agarose gel electrophoresis

Nucleic acid samples were loaded on 2% (w/v) agarose gel and then separated by electrophoresis in Tris-acetate-EDTA running buffer at 120 V for 30 min. Gel images were taken using the ChemiDoc MP imaging system (Bio-Rad, CA, USA).

CCK-8 assay

To understand the response of PDAC cells to GEM treatment, 5000 treated pancreatic cells per well were seeded in a 96-well plate. On the next day, fresh, GEM-containing medium was added to the cells at gradient concentrations of 0, 0.001, 0.01, 0.1, 1, 10, 100, and 1000 μM. After 48 h of incubation, the cells were incubated for 2 h at 37 °C with 10 μL CCK-8 solution (Dojindo, Japan). Absorbance was measured at 450 nm using a microplate reader (Tecan Trading AG, Switzerland). The IC50 value was calculated using GraphPad Prism 9.0 software to determine the extent of tumor cell response to GEM.

Colony formation assay

PDAC cells (800 cells per well) were added to 6-well plates and allowed to attach during incubation for 24 h. After treatment with GEM for 2 days, the medium was replaced with a complete medium, and the cells were cultured for 2 weeks. For counting after this period, colonies were fixed in 4% paraformaldehyde for 20 min and then stained with 0.1% crystal violet. The colonies were then counted manually. Three independent experiments were performed.

3D tumor microsphere live/dead staining

Tumor cells were washed three times with PBS, and then cell dissociation enzymes were added to obtain a single-cell suspension without clusters. The cell suspension was transferred to a sterile container and 200 μL/well was dispensed into Ultra Low Attachment (ULA) 96-well round-bottom plates (1500 cells/well) using a multichannel pipette. These plates were transferred to an incubator (37 °C, 5% CO2, 95% humidity) for growth. Three-day-old microsphere samples were treated with GEM for 48 h. Then cells were stained with a Live (Calcein-AM)/Dead (NucRed D) staining kit (BestBio, Shanghai, China), and images were obtained using an inverted fluorescence microscope.

Western blotting

Total proteins were extracted using radioimmunoprecipitation assay (RIPA) lysis buffer (Beyotime, China) containing protease inhibitors. Protein concentration was determined using the BCA method (Thermo Fisher Scientific, USA). Next, proteins were separated by sodium dodecyl sulfate (SDS)-polyacrylamide gel electrophoresis (PAGE) and then transferred onto polyvinylidene difluoride (PVDF) membranes. The membranes were blocked with 5% nonfat milk solution for 2 h at room temperature and then incubated overnight at 4 °C. The next day the appropriate primary antibody (RXRA (Cat. No. A19105, ABclonal, Boston, USA), CTSL (Cat. No. 66914-1-Ig, Proteintech, Chicago, USA), AKT1/2/3 (Cat. No. ET1609-51, HUABIO, Hanzhou, China), Phospho-AKT (ser473) (Cat. No. ET1607-73, HUABIO), Phospho-pan-AKT1/2/3 (Thr308) (Cat.No. AF3262, Affinity biosciences, Changzhou, China), GAPDH (Cat. No. ET1601-4, HUABIO), CSTB (Cat. No. sc-166561, Santa Cruz Biotechnology, USA), CSTA (Cat. No. ER63192, HUABIO), IGF2BP2 (Cat. No. HA720003, HUABIO), AGO2 (Cat. No. ET1702-39, HUABIO). solution was added, followed by incubation at room temperature for 1 h. After three washes with Tris-buffered saline containing Tween 20 (TBST), the targeted proteins were visualized using an enhanced chemiluminescence (ECL) reagent.

Immunohistochemistry (IHC) and H&E staining

For IHC analysis, tumor tissues were fixed in 4% paraformaldehyde and embedded in paraffin. Tissue sections were deparaffinized and rehydrated, followed by antigen retrieval through heat mediation in citrate buffer. Samples were blocked with 5% bovine serum albumin (BSA) for 1 h. Sections were incubated in primary antibody solutions overnight at 4 °C, followed by incubation with secondary antibody solution at room temperature for 1 h. A diaminobenzidine (DAB) solution was used to generate the chromogenic reaction.

Fluorescence in situ hybridization (FISH)

Fluorescently labeled cFAM124A probes were designed and synthesized by Servicebio (Wuhan, China). After fixation, permeabilization, and pre-hybridization, samples were hybridized with the probes in a hybridization buffer at 37 °C overnight. The hybridization buffer was then gradually washed away with 4× SSC (including 0.1% Tween-20), 2× SSC and 1× SSC at 42 °C. Cell nuclei were stained with DAPI.

Enzyme-linked immunosorbent assay (ELISA)

Cellular CTSL enzyme activity was measured using a human CTSL ELISA kit (Shanghai Enzyme-linked Biotechnology Co., Ltd.), according to the manufacturer's instructions. Briefly, 100 μl of cell lysate from the indicated PDAC lines was collected and incubated at 37℃ for 60 min. CTSL detection antibody, streptavidin-horseradish peroxidase (HRP), and tetramethylbenzidine (TMB) were added, and the intensity of the color was measured at 450 nm using as spectrophotometer.

RNA immunoprecipitation (RIP) assay

RIP was performed using the Magna RIP RNA Binding Protein Immunoprecipitation Kit (Merck Millipore, MA, USA) according to the manufacturer's protocol. Co-precipitated RNA was detected and analyzed by RT-qPCR.

Methylated RNA immunoprecipitation (MeRIP) assay

MeRIP analysis was performed using the Magna MeRIP m6A kit (Merck Millipore, MA, USA) according to the manufacturer's protocol. Co-precipitated RNA was detected and analyzed by RT- qPCR.

RNA antisense purification (RAP) assay

The RAP assay was performed using the BersinBio RNA Antisense Purification Kit (BersinBio, Guangzhou, China), according to the manufacturer's protocol. Co-precipitated proteins were detected and analyzed by western blotting using a silver staining kit (Solarbio, Beijing, China). Co-precipitated RNA was detected and analyzed by RT-qPCR.

Animal experiments

Balb/c nude mice (4–6 weeks old) were purchased from the Anburui BD Laboratory (Fuzhou, China). All animal procedures strictly followed the "Principles for the Use and Care of Vertebrates" and "Guidelines for the Care and Use of Experimental Animals." All animal experiments were approved by the Institutional Animal Care and Use Committee of Fujian Medical University (FPH. SL.20230606[0009], 2021-8CAARM153).

Orthotopic tumor model

PDOs were cultured in standard 6-well plates for 1 week and recovered in cold Hank's buffered saline solution (HBSS) as undissociated organoids. PDOs were then digested with a 10% fraction at 37 °C for 10 min and centrifuged at 600×g for 5 min at room temperature. PDO-derived cells were suspended in 100 µl HBSS with 50% BME, and then 1×10^6 cells per flank were injected into the parenchyma of the pancreas of nude mice. Five weeks later, tumor growth was evaluated by in vivo luciferase-based noninvasive bioluminescence imaging, and mice were euthanized after measurement.

Subcutaneous xenograft model

PDAC cells (5×10^6 cells in a 1:1 solution of PBS and Matrigel in a final volume of 100 µL per mouse) were subcutaneously injected into the left and right flanks of nude mice. Tumor volume was determined from measurements taken using electronic calipers and calculated as follows: volume (mm^3) = (W × L)/2, where W is the short axis and L is the long axis. The mice in each group ($n=5$) received intraperitoneal injections of saline or GEM (50 mg/kg) twice per week for 4 weeks with regular monitoring of tumor size, which reached approximately 3 mm in diameter. Six weeks later, all mice were euthanized.

RNA-Seq

Total RNA was extracted utilizing the Trizol reagent kit (Invitrogen, Carlsbad, CA, USA) per the manufacturer's protocol. The quality of the RNA was assessed using an Agilent 2100 Bioanalyzer (Agilent Technologies, Palo Alto, CA, USA) and verified through RNase-free agarose gel electrophoresis. Following the extraction of total RNA, eukaryotic mRNA was enriched using Oligo(dT) beads. The enriched mRNA was fragmented into smaller pieces with a fragmentation buffer and then reverse-transcribed into cDNA. The purified double-stranded cDNA fragments were subjected to end repair, addition of an A base, and ligation with Illumina sequencing adapters. The ligation reaction was purified using AMPure XP Beads (1.0X) and amplified via polymerase chain reaction (PCR). The resultant cDNA library was sequenced on the Illumina Novaseq6000 platform by Gene Denovo Biotechnology Co. (Guangzhou, China). The mapped reads from each sample were assembled using StringTie (version 1.3.1) in a reference-based approach. Normalization was performed using the DESeq2 pipeline, applying size factors for normalization. This method is part of the R Bioconductor package DESeq2. Differential expression analysis was carried out using the DESeq2 R package. The criteria for selecting genes for further analysis included an adjusted p-value threshold of <0.05 and a log2 fold change >1 or <-1.

Proteomics

Proteomics analysis of cell samples was conducted using a combination of data-dependent acquisition (DDA). Protein samples were obtained by FASP digestion of 100 µg cell lysate. Each sample was injected for nano-liquid chromatography (LC)- tandem mass spectrometry (MS/MS) analysis on a Q Executive HF-X mass spectrometer (Thermo Fisher Scientific) that was coupled to Easy nLC1200 (Thermo Fisher Scientific). MS data were acquired using a data-dependent top 10 method dynamically choosing the most abundant precursor ions from the survey scan (350–1800 m/z) for HCD fragmentation. MS2 scans were acquired at a resolution of 15,000 for HCD spectra at m/z 200 with an AGC target of 2e5 and a max IT of 60 ms, and isolation width was 2 m/z. The MS data were analyzed using MaxQuant software version 1.6.17.0. MS data were searched against the database (uniprot_homo). The cut-off of global false discovery rate (FDR) for peptide and protein identification was set to 0.01. Protein abundance was calculated based on the normalized spectral protein intensity (LFQ intensity). All results were filtered at a Q cut-off of 0.05 (equivalent

to a 1% false discovery rate). P-value estimation was performed by the Kernel density estimator.

Reagents

Gemcitabine (LY 188011), Nab-Paclitaxel (HY-P99974), K-80003 (HY-U00458), Copanlisib (HY-15346), Z-FY-CHO (HY-128140) and PD150606 (HY-100529) were purchased from MedChemExpress (Monmouth Junction, New Jersey, USA).

Statistical analysis

GraphPad Prism 9.0 and SPSS 26.0 were used for statistical analyses. Categorical variables were analyzed using Pearson's χ^2 statistic or Fisher's exact test. Comparisons among multiple groups were performed using a one-way analysis of variance (ANOVA). Student t-test was used to assess differences in data between the two groups. Overall survival (OS) and relapse-free survival (RFS) were assessed using the Kaplan–Meier method and compared using the log-rank test. P values <0.05 indicated differences were statistically significant ($^{*}P<0.05$, $^{**}P<0.01$, and $^{***}P<0.001$), and P values ≥ 0.05 indicated differences were non-significant (ns).

Supplementary Information

The online version contains supplementary material available at https://doi.org/10.1186/s12943-024-02128-2.

Supplementary Material 1

Supplementary Material 2

Author contributions

Shi Chen, Hui-Xing Chen and Li-Qun Chen designed the study. Cheng-Ke Xie and Cheng-Yu Liao performed the study and wrote the paper. Hong-Yi Lin conducted the experiments. Yong-Ding Wu and Feng-Chun Lu participated in data analysis. Xiao-Xiao Huang, Zu-Wei Wang, and Qiao-Wei Li assisted with experiments. Jian-Fei Hu and Cai-Feng Lin collected the tissues. Yin-Hao Chen, and Ge Li provided technical help. All authors read and approved the final manuscript. No potential conflicts of interest were disclosed. Cheng-Ke Xie was responsible for the reliability of all data.

Funding

This work was supported by the Major Scientific Research Project of Young and Middle-aged people of Fujian Provincial Health Commission (2021ZQNZD001, to Shi Chen), the Natural Science Foundation of Fujian Province of China (2020J011007, to Hui-Xing Chen), the Fujian Province Science and Technology Innovation Joint Fund Project (Shi Chen, 2023Y9334), the Fujian Research and Training Grants for Young and Middle-aged Leaders in Healthcare(No.2021(60), to Shi Chen), the Special Funding Project of Fujian Provincial Department of Finance (2100201, to Shi Chen). This work was sponsored by the Key Clinical Specialty Discipline Construction Program of Fujian, P.R.C. This work was supported by Geriatric Center Construction Program of Fujian Provincial Medical Creating Double-high Project. We thank the supports from Prof. Xiao-Kun Zhang of Xiamen University (Xiamen, China). And we thank the supports from Prof. Guo-Zhong Liu of The First Affiliated Hospital of Fujian Medical University (Fuzhou, China). We also thank the technical supports from Panomix Biomedical Tech Co., Ltd. (Suzhou, China), the Anburui BD Laboratory (Fuzhou, China), Gene Denovo Biotechnology Co., Ltd. (Guangzhou, China), Shanghai Outdo Biotech Company (Shanghai, China), GeneChem Co., Ltd. (Shanghai, China), Fuzhou Sunya Biotechnology Co., Ltd. (Fuzhou, China), Servicebio (Wuhan, China), AimingMed Technologies Co., Ltd. (Hangzhou, China) and Keystone Biotechnology Co., Ltd. (Fuzhou, China). Fig. 1A, Fig. 1I, Fig. 2A, Fig. 3A, Fig. 3E, Fig. 3G, Fig. 4A, Fig. 7K and Fig. 8K were Created with BioRender.com released under a Creative Commons Attribution-NonCommercial-NoDerivs 4.0 International license (https://creativecommons.org/licenses/by-nc-nd/4.0/deed.en).

Data availability

The datasets used and analyzed during the current study are available from the correspondingauthor upon reasonable request.

Declarations

Competing interests

The authors declare no competing interests.

Ethical approval

This study was authorized (FPH.SL.20230606[0009], K2021-08-004) by the Ethics Committee of Fujian Provincial Hospital (Fuzhou, China). All animals were handled strictly according to the Principles for the Utilization and Care of Vertebrate Animals and the Guide for the Care and Use of Laboratory Animals. All animal experiments were approved by the Institutional Animal Care and Use Committee of Fujian Medical University (2021-8CAARM153).

Author details

[1]Shengli Clinical Medical College of Fujian Medical University, Fuzhou 350001, China
[2]Department of Hepatobiliary Pancreatic Surgery, Fuzhou University Affiliated Provincial Hospital, Fujian Provincial Hospital, Fuzhou 350001, China
[3]Fuzhou University, Fuzhou 350001, China
[4]Department of Hepatobiliary Surgery, Fujian Institute of Hepatobiliary Surgery, Fujian Medical University Union Hospital, Fuzhou 350001, China
[5]Fujian Provincial Center for Geriatrics, Fuzhou 350001, China
[6]Fujian Key Laboratory of Geriatrics, Fuzhou 350001, China
[7]College of Biological Science and Engineering, Fuzhou University, Fuzhou 350108, China
[8]Fujian Medical University Cancer Center, Fuzhou 350001, China
[9]Institute of Applied Genomics, Fuzhou University, Fuzhou 350108, China
[10]Department of General Surgery, Fujian Medical University Union Hospital, Fuzhou 350001, China

Received: 6 August 2024 / Accepted: 18 September 2024
Published online: 30 September 2024

References

1. Siegel RL, Miller KD, Wagle NS, Jemal A. Cancer statistics, 2023. CA Cancer J Clin. 2023;73:17–48.
2. Strobel O, Neoptolemos J, Jäger D, Büchler MW. Optimizing the outcomes of pancreatic cancer surgery. Nat Rev Clin Oncol. 2019;16:11–26.
3. Hackert T, Sachsenmaier M, Hinz U, Schneider L, Michalski CW, Springfeld C, Strobel O, Jäger D, Ulrich A, Büchler MW. Locally Advanced Pancreatic Cancer: Neoadjuvant Therapy with Folfirinox results in Resectability in 60% of the patients. Ann Surg. 2016;264:457–63.
4. Gemenetzis G, Groot VP, Blair AB, Laheru DA, Zheng L, Narang AK, Fishman EK, Hruban RH, Yu J, Burkhart RA, et al. Survival in locally Advanced Pancreatic Cancer after Neoadjuvant Therapy and Surgical Resection. Ann Surg. 2019;270:340–7.
5. Barenboim A, Lahat G, Geva R, Nachmany I, Nakache R, Goykhman Y, Brazowski E, Rosen G, Isakov O, Wolf I, et al. Neoadjuvant FOLFIRINOX for locally advanced and borderline resectable pancreatic cancer: an intention to treat analysis. Eur J Surg Oncol. 2018;44:1619–23.
6. Miyasaka Y, Ohtsuka T, Kimura R, Matsuda R, Mori Y, Nakata K, Kakihara D, Fujimori N, Ohno T, Oda Y, Nakamura M. Neoadjuvant Chemotherapy with Gemcitabine Plus Nab-Paclitaxel for Borderline Resectable Pancreatic Cancer potentially improves survival and facilitates surgery. Ann Surg Oncol. 2019;26:1528–34.
7. De Jesus-Acosta A, Sugar EA, O'Dwyer PJ, Ramanathan RK, Von Hoff DD, Rasheed Z, Zheng L, Begum A, Anders R, Maitra A, et al. Phase 2 study of vismodegib, a hedgehog inhibitor, combined with gemcitabine and

nab-paclitaxel in patients with untreated metastatic pancreatic adenocarcinoma. Br J Cancer. 2020;122:498–505.
8. Jiang L, Qin J, Dai Y, Zhao S, Zhan Q, Cui P, Ren L, Wang X, Zhang R, Gao C, et al. Prospective observational study on biomarkers of response in pancreatic ductal adenocarcinoma. Nat Med. 2024;30:749–61.
9. Marabelle A, Le DT, Ascierto PA, Di Giacomo AM, De Jesus-Acosta A, Delord JP, Geva R, Gottfried M, Penel N, Hansen AR, et al. Efficacy of Pembrolizumab in patients with Noncolorectal high microsatellite Instability/Mismatch repair-deficient Cancer: results from the phase II KEYNOTE-158 study. J Clin Oncol. 2020;38:1–10.
10. Galluzzi L, Humeau J, Buqué A, Zitvogel L, Kroemer G. Immunostimulation with chemotherapy in the era of immune checkpoint inhibitors. Nat Rev Clin Oncol. 2020;17:725–41.
11. Peng J, Sun BF, Chen CY, Zhou JY, Chen YS, Chen H, Liu L, Huang D, Jiang J, Cui GS, et al. Single-cell RNA-seq highlights intra-tumoral heterogeneity and malignant progression in pancreatic ductal adenocarcinoma. Cell Res. 2019;29:725–38.
12. Connor AA, Gallinger S. Pancreatic cancer evolution and heterogeneity: integrating omics and clinical data. Nat Rev Cancer. 2022;22:131–42.
13. Glaviano A, Foo ASC, Lam HY, Yap KCH, Jacot W, Jones RH, Eng H, Nair MG, Makvandi P, Geoerger B, et al. PI3K/AKT/mTOR signaling transduction pathway and targeted therapies in cancer. Mol Cancer. 2023;22:138.
14. Jin Y, Chen Y, Tang H, Hu X, Hubert SM, Li Q, Su D, Xu H, Fan Y, Yu X, et al. Activation of PI3K/AKT pathway is a potential mechanism of Treatment Resistance in Small Cell Lung Cancer. Clin Cancer Res. 2022;28:526–39.
15. Conway JR, Herrmann D, Evans TJ, Morton JP, Timpson P. Combating pancreatic cancer with PI3K pathway inhibitors in the era of personalised medicine. Gut. 2019;68:742–58.
16. Baselga J, Campone M, Piccart M, Burris HA 3rd, Rugo HS, Sahmoud T, Noguchi S, Gnant M, Pritchard KI, Lebrun F, et al. Everolimus in postmenopausal hormone-receptor-positive advanced breast cancer. N Engl J Med. 2012;366:520–9.
17. Kim HR, Kang HN, Yun MR, Ju KY, Choi JW, Jung DM, Pyo KH, Hong MH, Ahn MJ, Sun JM, et al. Mouse-human co-clinical trials demonstrate superior anti-tumour effects of buparlisib (BKM120) and cetuximab combination in squamous cell carcinoma of head and neck. Br J Cancer. 2020;123:1720–9.
18. Das M. Duvelisib in indolent non-hodgkin lymphoma. Lancet Oncol. 2019;20:e138.
19. Peng T, Dou QP. Everolimus inhibits growth of Gemcitabine-resistant pancreatic Cancer cells via induction of caspase-dependent apoptosis and G(2) /M arrest. J Cell Biochem. 2017;118:2722–30.
20. Cui J, Guo Y, Wu H, Xiong J, Peng T. Everolimus regulates the activity of gemcitabine-resistant pancreatic cancer cells by targeting the Warburg effect via PI3K/AKT/mTOR signaling. Mol Med. 2021;27:38.
21. Ito D, Fujimoto K, Mori T, Kami K, Koizumi M, Toyoda E, Kawaguchi Y, Doi R. In vivo antitumor effect of the mTOR inhibitor CCI-779 and gemcitabine in xenograft models of human pancreatic cancer. Int J Cancer. 2006;118:2337–43.
22. Wolpin BM, Hezel AF, Abrams T, Blaszkowsky LS, Meyerhardt JA, Chan JA, Enzinger PC, Allen B, Clark JW, Ryan DP, Fuchs CS. Oral mTOR inhibitor everolimus in patients with gemcitabine-refractory metastatic pancreatic cancer. J Clin Oncol. 2009;27:193–8.
23. Kordes S, Richel DJ, Klümpen HJ, Weterman MJ, Stevens AJ, Wilmink JW. A phase I/II, non-randomized, feasibility/safety and efficacy study of the combination of everolimus, cetuximab and capecitabine in patients with advanced pancreatic cancer. Invest New Drugs. 2013;31:85–91.
24. Qi WX, Huang YJ, Yao Y, Shen Z, Min DL. Incidence and risk of treatment-related mortality with mTOR inhibitors everolimus and temsirolimus in cancer patients: a meta-analysis. PLoS ONE. 2013;8:e65166.
25. Zhu J, Naulaerts S, Boudhan L, Martin M, Gatto L. Van den Eynde BJ: Tumour immune rejection triggered by activation of α2-adrenergic receptors. Nature. 2023;618:607–15.
26. Tan XP, He Y, Yang J, Wei X, Fan YL, Zhang GG, Zhu YD, Li ZQ, Liao HX, Qin DJ, et al. Blockade of NMT1 enzymatic activity inhibits N-myristoylation of VILIP3 protein and suppresses liver cancer progression. Signal Transduct Target Ther. 2023;8:14.
27. Meng J, Han J, Wang X, Wu T, Zhang H, An H, Qin L, Sun Y, Zhong W, Yang C, et al. Twist1-YY1-p300 complex promotes the malignant progression of HCC through activation of miR-9 by forming phase-separated condensates at super-enhancers and relieved by metformin. Pharmacol Res. 2023;188:106661.
28. Zhou H, Liu W, Su Y, Wei Z, Liu J, Kolluri SK, Wu H, Cao Y, Chen J, Wu Y, et al. NSAID sulindac and its analog bind RXRalpha and inhibit RXRalpha-dependent AKT signaling. Cancer Cell. 2010;17:560–73.
29. Ye X, Wu H, Sheng L, Liu YX, Ye F, Wang M, Zhou H, Su Y, Zhang XK. Oncogenic potential of truncated RXRα during colitis-associated colorectal tumorigenesis by promoting IL-6-STAT3 signaling. Nat Commun. 2019;10:1463.
30. Aufiero S, Reckman YJ, Pinto YM, Creemers EE. Circular RNAs open a new chapter in cardiovascular biology. Nat Rev Cardiol. 2019;16:503–14.
31. Vo JN, Cieslik M, Zhang Y, Shukla S, Xiao L, Zhang Y, Wu YM, Dhanasekaran SM, Engelke CG, Cao X, et al. The Landscape of circular RNA in Cancer. Cell. 2019;176:869–e881813.
32. Chen ZW, Hu JF, Wang ZW, Liao CY, Kang FP, Lin CF, Huang Y, Huang L, Tian YF, Chen S. Circular RNA circ-MTHFD1L induces HR repair to promote gemcitabine resistance via the miR-615-3p/RPN6 axis in pancreatic ductal adenocarcinoma. J Exp Clin Cancer Res. 2022;41:153.
33. Wang ZW, Pan JJ, Hu JF, Zhang JQ, Huang L, Huang Y, Liao CY, Yang C, Chen ZW, Wang YD, et al. SRSF3-mediated regulation of N6-methyladenosine modification-related lncRNA ANRIL splicing promotes resistance of pancreatic cancer to gemcitabine. Cell Rep. 2022;39:110813.
34. Liu Z, Gu S, Wu K, Li L, Dong C, Wang W, Zhou Y. CircRNA-DOPEY2 enhances the chemosensitivity of esophageal cancer cells by inhibiting CPEB4-mediated Mcl-1 translation. J Exp Clin Cancer Res. 2021;40:361.
35. Wang X, Chen T, Li C, Li W, Zhou X, Li Y, Luo D, Zhang N, Chen B, Wang L, et al. CircRNA-CREIT inhibits stress granule assembly and overcomes doxorubicin resistance in TNBC by destabilizing PKR. J Hematol Oncol. 2022;15:122.
36. Daamen LA, Groot VP, Goense L, Wessels FJ, Borel Rinkes IH, Intven MPW, van Santvoort HC, Molenaar IQ. The diagnostic performance of CT versus FDG PET-CT for the detection of recurrent pancreatic cancer: a systematic review and meta-analysis. Eur J Radiol. 2018;106:128–36.
37. Chen H, Li F, Zou S, Xie J, Zhang J, Deng X, Chen H, Shen B. Preoperative plasma D-dimer independently predicts survival in patients with pancreatic ductal adenocarcinoma undergoing radical resection. World J Surg Oncol. 2021;19:166.
38. Yang G, Guan W, Cao Z, Guo W, Xiong G, Zhao F, Feng M, Qiu J, Liu Y, Zhang MQ, et al. Integrative Genomic Analysis of Gemcitabine Resistance in Pancreatic Cancer by patient-derived xenograft models. Clin Cancer Res. 2021;27:3383–96.
39. Biankin AV, Waddell N, Kassahn KS, Gingras MC, Muthuswamy LB, Johns AL, Miller DK, Wilson PJ, Patch AM, Wu J, et al. Pancreatic cancer genomes reveal aberrations in axon guidance pathway genes. Nature. 2012;491:399–405.
40. Jiang X, Ma Y, Wang T, Zhou H, Wang K, Shi W, Qin L, Guan J, Li L, Long B, et al. Targeting UBE2T potentiates Gemcitabine Efficacy in Pancreatic Cancer by regulating pyrimidine metabolism and replication stress. Gastroenterology. 2023;164:1232–47.
41. Chen L, Aleshin AE, Alitongbieke G, Zhou Y, Zhang X, Ye X, Hu M, Ren G, Chen Z, Ma Y, et al. Modulation of nongenomic activation of PI3K signalling by tetramerization of N-terminally-cleaved RXRα. Nat Commun. 2017;8:16066.
42. Kristensen LS, Jakobsen T, Hager H, Kjems J. The emerging roles of circRNAs in cancer and oncology. Nat Rev Clin Oncol. 2022;19:188–206.
43. Ciechanover A. The unravelling of the ubiquitin system. Nat Rev Mol Cell Biol. 2015;16:322–4.
44. Gao W, Liu J, Hu M, Huang M, Cai S, Zeng Z, Lin B, Cao X, Chen J, Zeng JZ, et al. Regulation of proteolytic cleavage of retinoid X receptor-α by GSK-3β. Carcinogenesis. 2013;34:1208–15.
45. Nomura Y, Nagaya T, Yamaguchi S, Katunuma N, Seo H. Cleavage of RXRalpha by a lysosomal enzyme, cathepsin L-type protease. Biochem Biophys Res Commun. 1999;254:388–94.
46. Zhong Y, Du Y, Yang X, Mo Y, Fan C, Xiong F, Ren D, Ye X, Li C, Wang Y, et al. Circular RNAs function as ceRNAs to regulate and control human cancer progression. Mol Cancer. 2018;17:79.
47. Huang H, Weng H, Sun W, Qin X, Shi H, Wu H, Zhao BS, Mesquita A, Liu C, Yuan CL, et al. Recognition of RNA N(6)-methyladenosine by IGF2BP proteins enhances mRNA stability and translation. Nat Cell Biol. 2018;20:285–95.
48. Kos J, Lah TT. Cysteine proteinases and their endogenous inhibitors: target proteins for prognosis, diagnosis and therapy in cancer (review). Oncol Rep. 1998;5:1349–61.
49. Gu J, Huang W, Wang X, Zhang J, Tao T, Zheng Y, Liu S, Yang J, Chen ZS, Cai CY, et al. Hsa-miR-3178/RhoB/PI3K/Akt, a novel signaling pathway regulates ABC transporters to reverse gemcitabine resistance in pancreatic cancer. Mol Cancer. 2022;21:112.

50. Chen SY, Hsu YH, Wang SY, Chen YY, Hong CJ, Yen GC. Lucidone inhibits autophagy and MDR1 via HMGB1/RAGE/PI3K/Akt signaling pathway in pancreatic cancer cells. Phytother Res. 2022;36:1664–77.
51. Chaves-Almagro C, Auriau J, Dortignac A, Clerc P, Lulka H, Deleruyelle S, Projetti F, Nakhlé J, Frances A, Berta J et al. Upregulated Apelin Signaling in Pancreatic Cancer activates Oncogenic Signaling pathways to promote Tumor Development. Int J Mol Sci 2022, 23.
52. Manning BD, Cantley LC. AKT/PKB signaling: navigating downstream. Cell. 2007;129:1261–74.
53. Zhai S, Lin J, Ji Y, Zhang R, Zhang Z, Cao Y, Liu Y, Tang X, Liu J, Liu P, et al. A microprotein N1DARP encoded by LINC00261 promotes Notch1 intracellular domain (N1ICD) degradation via disrupting USP10-N1ICD interaction to inhibit chemoresistance in Notch1-hyperactivated pancreatic cancer. Cell Discov. 2023;9:95.
54. Liu CX, Chen LL. Circular RNAs: characterization, cellular roles, and applications. Cell. 2022;185:2016–34.
55. Li B, Zhu L, Lu C, Wang C, Wang H, Jin H, Ma X, Cheng Z, Yu C, Wang S, et al. circNDUFB2 inhibits non-small cell lung cancer progression via destabilizing IGF2BPs and activating anti-tumor immunity. Nat Commun. 2021;12:295.
56. Pan X, Huang B, Ma Q, Ren J, Liu Y, Wang C, Zhang D, Fu J, Ran L, Yu T, et al. Circular RNA circ-TNPO3 inhibits clear cell renal cell carcinoma metastasis by binding to IGF2BP2 and destabilizing SERPINH1 mRNA. Clin Transl Med. 2022;12:e994.

Publisher's note